An analysis of spark chamber operation

Burnham, J. U.

An Analysis of Spark Chamber Operation

by J.U. Burnham, B.Sc.

A thesis submitted to the University of Durham, as an application for the degree of Master of Science

September, 1963.

Frontispiece: Spark chamber in a magnetic field showing electron cascades produced by 1.3 GeV/c π^- beam.

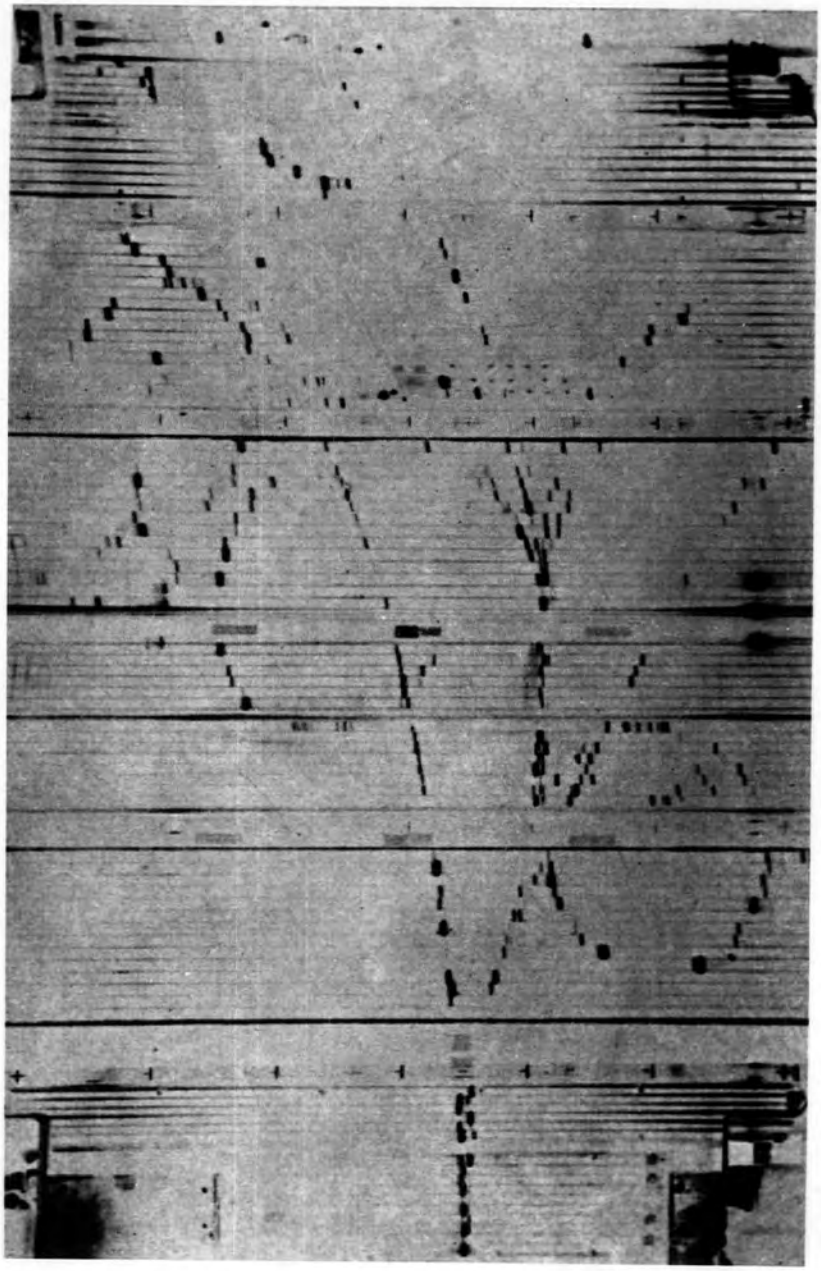

Preface

The work described in this thesis has been carried out in the Physics Department of the University of Durham under the supervision of Dr. A.W. Wolfendale during the period from October, 1961, to September, 1963. The author was the recipient of a D.S.I.R. Advanced Course Studentship.

He was responsible for the design, construction, and operation of the apparatus described in this thesis. The analysis of the data was the author's responsibility, and he also contributed a major part to the development of the theory. The responsibility for the accuracy of the historical review and the survey of the different types of spark chamber given in this thesis rests with the author.

Some of the results presented in sections 4.1 and 4.2 of this thesis have been published by the author and his colleagues ("An analysis of the characteristics of a neon-alcohol spark chamber" by Burnham, J.U., Rogers, I.W., Thompson, M.G., and Wolfendale, A.W.) in J. Sci. Instrum., 1963, 40, 296. Further results on electron attachment are being prepared for submission for publication in the same journal ("Electron attachment in a neon spark chamber" by Burnham, J.U. and Thompson, M.G.).

Abstract

The characteristics of a spark chamber containing a neon-alcohol mixture are described with particular reference to the variation of efficiency with the parameters of the pulse and the determination of the spark formation time. An interpretation is made on the basis of a model for spark formation and the validity of the mechanism is examined by an internal comparison of the data.

The results are used to derive the electron drift velocity as a function of field over the range of E/p from 0.05 to 4 v $cm^{-1}(mm\ Hg)^{-1}$ and to determine the probability of a single electron initiating a spark. This is found to be 0.25.

Measurements are also reported on the effect of electron attachment and on the geometrical properties of the sparks. Conditions are studied both for minimising the angle between the direction of the particle trajectory and the ensuing spark, and for reducing the error in location of the trajectory (0.2 mm).

Conclusions on the design of spark chambers are presented and a historical review of the development of the spark chamber as well as a survey of the different types of spark chambers developed up to the present time are given.

CONTENTS

List of Figures

Figure no.	Title
15	The efficiency as a function of T_D for the case of the clearing field in the opposite direction to the pulse field.
16	The time delay (T_{DO}) in which the efficiency falls to zero as a function of E^{-1} for E_C in opposition to the pulse field.
17	Universal relation between efficiency and the product of T_D and E_C in the same direction as the pulse field.
18	Universal relation between efficiency and the product of T_D and E_c for E_c in opposition to the pulse field.
19	Drift velocities of electrons as a function of E/p.
20	Frequency distributions of $\tan\theta_{1i}$ for a fixed $\tan\theta$ for two pulses.
21	The mean value of $\tan\theta_1$ (for each particle) as a function of $\tan\theta$.
22	The width of the spark as a function of the angle of the trajectory for various amplitudes and rise times.
23	Frequency distribution of δ, the displacement of the spark discharge from the estimated particle trajectory.
24	Geometrical property of the spark.
25	A single particle traversing the chamber.
26	A single particle.
27	A particle scattered in the aluminium plates of the chamber.
28	A knock-on electron produced by the cosmic ray particle is seen in the lowest two gaps.

Figure no.	Title
29	A knock-on electron produced in the first electrode.
30	Track of a single particle.
31	A knock-on electron produced in the third gap.
32	A cosmic ray shower event in which three particles traversed the chamber simultaneously.
33	The efficiency as a function of the time delay for various impurity concentrations.
34	The efficiency function $\ell n \left\{ \ell n \frac{1}{1-\eta} + 0.166 \sqrt{10^6 T_D} \right\}$ plotted against the impurity concentrations with T_D as parameter.
35	The gradients, s, of the straight lines of fig. 34 plotted against $1.32 \times 10^9 \ (T_D - 0.5 \times 10^{-6})$.
36	Chambers constructed by Rutherglen using a simple O-ring method.
37	Typical pulse generator circuit.
38	Three methods of photography.
39	Cylindrical spark chamber constructed by the Berkeley group.
40	Typical cosmic ray track obtained with a microwave spark chamber.

CHAPTER 1

A historical introduction of the development of the spark chamber up to 1961

1.1 General

Instruments for studying cosmic rays and nuclear particles can generally be divided into three main groups.

The first of these comprises electrical methods, in which the passage of an ionising particle through the detector initiates some form of electrical signal. Examples of this group are the ionisation chamber and the Geiger counter.

The second group includes such detectors as cloud chambers and nuclear emulsion, in which the actual particle trajectory is rendered visible over a limited space.

In the third group, detectors such as the spark counter and the spark chamber are classified. These give both an electrical signal and a visual record of the particle trajectory. The spark chamber in particular has become a powerful tool in experimental high energy nuclear physics. It is with this technique that the present thesis is concerned; its development from the earlier spark counter is briefly outlined below, and this is followed by a more detailed discussion of the technique.

1.2 The Development of the Spark Counter

The spark counter may be defined as any arrangement of electrodes operated in a gas atmosphere with a high static potential between them.

The first working spark counter appears to have been constructed by Greinacher (1936). This consisted of a point-plate electrode system, in air, to which a static potential difference just below the break-down potential was applied. On the traversal of a heavily ionising α-particle between the electrodes a spark discharge was initiated.

It was not until nine years later that further work on this type of counter was reported. Chang and Rosenblum (1945) constructed an α-particle counting system comprising several parallel-wire spark counters. The electrodes, which were operated in an atmosphere of air, consisted of eight very thin tungsten wires mounted parallel to a flat brass plate. The authors carefully investigated the conditions for reliable operation of these counters, which were capable of counting 600 α-particles per minute.

Keuffel (1948) was the first to introduce a parallel-plate spark counter. This was of great interest to investigators then searching for a detector with a fast response time, because parallel plate geometry provided a field everywhere uniform and consequently the shortest transit times.

Madansky and Pidd (1948), (1949), (1950) showed that such a counter avoided the random delay errors inherent in counters with cylindrical geometry and was suitable for measurements of life-times as short as 10^{-9} secs.

After initiation by an ionising particle the discharge produced in a parallel-plate spark counter would have persisted, unless external electronic quenching circuits were employed. It was noticed that if the overvoltage was restored too soon, spurious discharges occurred. With optimum cathode material these spurious pulses placed a lower limit of about one millisecond on the recovery times.

Keuffel (1949) noticed that the discharge in a parallel-plate spark counter was located actually on the trajectory of the charged particle traversing the counter. He pointed out that this was a way of determining particle tracks.

Bella and Franzinetti (1953a,b) repeated Keuffel's observations and pointed out that the position of an ionising particle could be located to within one cubic millimeter. Bella et al. (1953) published the first photographs of the spark discharge.

From this work Conversi and Gozzini (1955) and Conversi et al. (1956) developed the flash tube hodoscope. This consisted of an array of small glass tubes filled with neon and mounted between plane parallel electrodes. When an ionising particle had passed through a number of tubes, a suitable high voltage pulse was

applied across the plates, causing these tubes to flash with such intensity that a photographic record could easily be made. The major disadvantage of this detector was its limited ability to resolve high particle densities, since a particular flash tube gives the same record for one or more particles traversing it. Nevertheless, large arrays of neon flash tubes were built by Coxell and Wolfendale (1960) such that many particles could be recorded. The flash-tube hodoscope might well have found many applications in high-energy physics had it not been for the rapid development of the spark chamber.

Henning (1955) effected improvements to the spark counter technique by:

1. using several parallel-plate spark counters vertically above each other,
2. enhancing the spark intensity with a coincidence-triggered condenser discharge through the counter which enabled him to optically discriminate between selected and unselected particles,
3. taking stereo photographs.

Henning made the first measurements on the accuracy of track location and found that the error distribution could be resolved into three superposed gaussian distributions:-

a) 78% with standard deviation 0.8 mm.

b) 17% with standard deviation 7 mm.

c) 5% with standard deviation 25 mm.

Group b) was ascribed to secondary avalanches and to knock-on electrons, and group c) to multiple avalanche discharges and cosmic ray showers. These counters were filled with an argon-vapour mixture and, similar to air filled counters, were not suitable for recording the passage of more than one simultaneous ionising particle, because they depend on processes of attachment and subsequent detachment of the initial electrons produced by the ionising particle.

A considerable number of additional papers by Henning's colleagues in Hamburg (now at Kiel) followed up this work:- Bagge and Allkofer (1957), Allkofer et al. (1957), Bagge and Schmieder (1959), Allkofer (1959), Trumper (1960), and Allkofer (1960).

Cranshaw and de Beer (1957) combined the techniques of the flash-tube hodoscope and the spark counter by applying a high voltage pulse instead of a high D.C. field to the electrodes of a parallel plate spark counter. Only a small clearing potential was left between the plates to clear out any ions which may have been left after a discharge. Cranshaw and de Beer used air at atmospheric pressure, thus circumventing any problems of gas-tight enclosures, and facilitating the use of very cheaply constructed multiplate assemblies. Triggered spark counter arrays of large area for experiments on very high energy cosmic ray particles were used by de Beer (1960) in South Africa and by Mistry et al. (1960) in India.

1.3 The Development of the Spark Chamber

1.3a The Contribution of Fukui and Miyamoto

The major effort was now directed towards devising methods for observing the simultaneous passage of several ionising particles. The crucial step was taken by Fukui and Miyamoto (1959) who demonstrated that if, instead of air, a suitable mixture of neon and argon was used, a parallel-plate chamber would record the passage of more than one simultaneous particle providing that a high voltage pulse were applied immediately afterwards. A detector of this kind is now called a "spark chamber".

Fukui and Miyamoto were also the first to use the chamber as a track-following device, in which the discharge actually follows the track. They allowed particles to pass through the chamber in a direction parallel to the plane of the plates, and found that a discharge between the plates took place, localised along the track of the particles in sparks separated on the average by a few millimeters.

The developments of Fukui and Miyamoto promoted wide-spread interest in the potential usefulness of the chamber in experimental high energy nuclear physics.

1.3b The method of operation

Before outlining further developments of the spark chamber, it seems appropriate to describe briefly its method of operation.

The passage of an ionising particle through the chamber is detected by two scintillation counters coupled to photo-multipliers, whose output is fed into a coincidence circuit. The transmitted pulse triggers a high voltage pulse generator which supplies a pulse of several kilovolts to alternate plates of the chamber. The amplitude of this pulse is well above the D.C. breakdown potential of the gas in the chamber such that the electrons produced in it by the ionising particle initiate electron avalanches, which finally culminate in a luminous spark channel very close to the particle trajectory. The chamber can be made to have a very short sensitive time by maintaining a steady D.C. clearing field between the electrodes. For example a 100 volt clearing field applied to a 1 cm gap sweeps out the electrons produced by the ionising particle in approximately 1 μsec. Consequently if the chamber is pulsed more than 1 μsec after the passage of the particle no sparks will occur. This means the chamber can be set up in a beam of 10^6 particles/sec and a selective counter system may be employed to trigger the chamber only on those particles for which a visual record or spatial information is required.

The number of groups working on or with spark chambers has now become very large and therefore a summary of the vast amount of work done on spark chambers up to 1961 will necessarily be

sketchy. It will be more comprehensible to the reader to outline the work done on spark chambers under appropriate sub-headings concerning the different properties, rather than in a chronological order.

1.3c The Sensitive Time

The efficiency per gap of a spark chamber at a specific time delay (the time that elapses between the passage of the triggering particle through the chamber and the application of the high voltage pulse) depends on the magnitude of the clearing field across the gap. Fig. 1, given by Beall et al. (1960), shows the efficiency of a $\frac{1}{4}$ inch gap in 1 atmosphere of argon as a function of the time delay for various values of the clearing field applied in a direction opposite to the high voltage pulse. It can be seen that the sensitive time may be adjusted by the choice of suitable values of the clearing field.

Cronin and Renninger (1960) plotted a similar curve at the beginning of operation of their spark chamber, which was filled with research-grade neon, and after 10^5 pulses. They found that in each case there existed a clearing field for which the sensitive time was a minimum, and that this minimum changed from 1.3 μsec to 0.5 μsec after 10^5 pulses. No other workers using neon or argon fillings have observed a minimum in the sensitive time.

Culligan et al. (1960) have demonstrated that with argon sensitive times of 0.3 μsecs are obtainable. Their measurements were made with a 4 mm single gap chamber. Their curves for argon

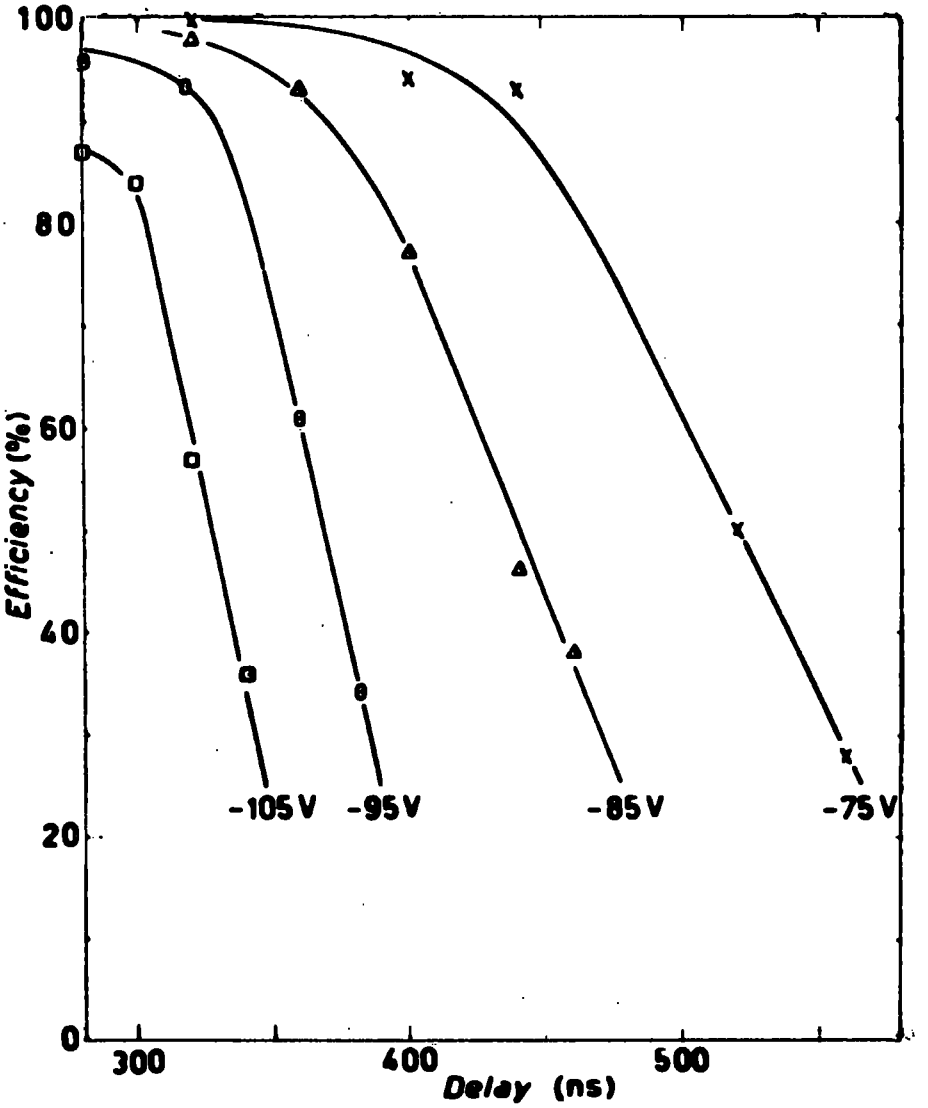

Efficiency of a single ½ in. gap in 1 atm of argon as a function of delay in application of the high-voltage pulse. The zero of the delay axis is the time at which the particle passed through the chamber.

Figure 1.

showed a long low efficiency tail, which was found to be eliminated by the addition of alcohol to the argon filling.

An alternative way of decreasing the sensitive time is to introduce small additives of electronegative impurity to the chamber filling. The effect is most probably due to attachment of the electrons, so that they are no longer able to initiate avalanches. Beall et al. (1960) found that the addition of $\frac{1}{2}\%$ oxygen or 5% CO_2 did not affect the efficiency appreciably with a time delay of 0.3 μsecs, but that greater quantities did reduce the efficiency.

1.3d The Electric Field Characteristics

One of the basic parameters of spark chambers is the time required for the formation of the spark measured from the instant of application of the high voltage pulse. Fischer and Zorn (1961) investigated the spark formation time as a function of pulse voltage under various conditions of electrode material, gap widths, gas fillings, delay times and clearing fields. Their results are shown in Fig. 2. The calculated curves are based on the theory of Dickey (1952), i.e. it is assumed that on application of the high voltage pulse the ionisation increases exponentially with time until

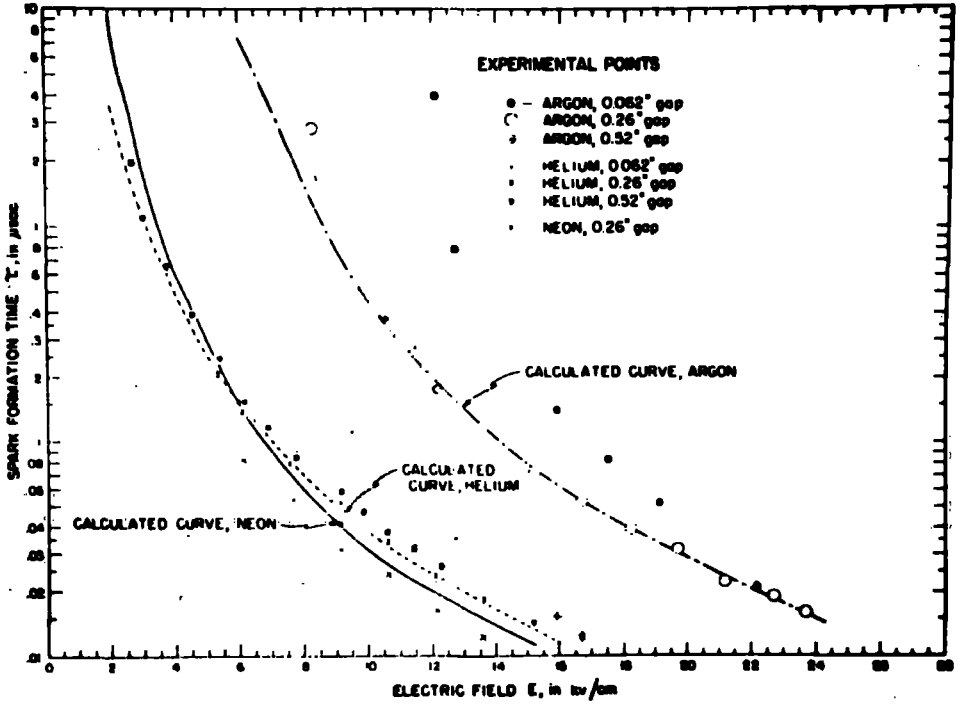

Figure 2. Comparison of the calculated and observed spark formation times as a function of the applied field for different gap widths.

the voltage across the gap is significantly reduced by the presence of the space charge. Fischer and Zorn showed that this criterion leads to a relationship for the spark formation time given by

$$T_F = \frac{29.5 \pm 0.5}{\alpha v} \text{ sec.}$$

where α is Townsend's first ionisation coefficient, which is the number of electrons produced per cm path by each electron, and v is the average drift velocity in cm/sec of the electrons in the applied field. The quoted uncertainty represents the maximum deviation for the three gases helium, neon and argon over the range of voltage used in their experiment. They observed variations of $\pm 10\%$ in the individual measured spark formation times. The following general characteristics were deduced from Fig. 2:-

a) The spark formation time decreases rapidly over several orders of magnitude with increasing pulse heights and is different for each gas.

b) The addition of alcohol results in curves which are displaced towards shorter spark formation times for argon and towards longer times for helium.

Fischer and Zorn also found that the introduction of delay times and the application of clearing fields did not produce any significant change in spark formation times, and that any conducting material with a relatively smooth finish may be used for the plates.

Helium, neon, argon and mixtures of these gases have all been used in spark chambers. Typical pulse heights for satisfactory operation at one atmosphere of pressure are ~8 kv/cm for neon and helium and ~16 kv/cm for argon.

1.3e The Recovery Time

The recovery time is the relatively long interval which must elapse before the chamber is ready to be used again.

Fischer and Zorn (1961) found that when a chamber was artificially re-pulsed at some time after it had recorded the track of an ionising particle, the old track was re-ignited for times up to 0.5 msec in neon and 1 msec in argon. For longer delays sparks were still observed, but not necessarily on the old track. No sparks were seen when the chamber was repulsed 100 msec after the traversal of the ionising particle. They also showed that even if an old track was re-ignited it was possible to see a new particle track at the same time.

The addition of a quenching agent, such as alcohol, reduced the probability of re-ignition; for example Culligan et al. (1960) found that in an argon-alcohol mixture the recovery time was less then 1 msec.

1.3f The Accuracy of Track Location

Detailed studies of the accuracy with which the sparks define the path of a triggering particle have been made by Mikhailov et al. (see Alikhanian and Kozodaev, 1960) and Rutherglen and Paterson (1961).

It was found that the sparks tend to follow the electric field direction rather than the particle track direction. For an angled track it was therefore important to know which part of the spark would most likely indicate the position of the track. Mikhailov et al. found that the optimum point on the spark for measurement lay at a distance 0.16 d from the cathode, where d is the gap width, and Rutherglen and Paterson found this point to be situated at a distance 0.2 d from the cathode. These results were obtained with zero clearing field. When a clearing field is applied the electrons moving normally to the plates also cause this alignment point to move relative to the track.

The results of Rutherglen and Paterson for the deviations of sparks from the tracks defined in the above way are tabulated in table 1.

TABLE 1

Track Direction relative to the normal to the plates	R.M.S. Deviation
0 - 15°	0.25 mm
15 - 30°	0.5 mm
30 - 45°	0.8 mm

These results were obtained in a mixture of 75% He and 25% Argon with d = $\frac{1}{4}$" and a time delay of 0.25 μsec.

They found that the application of a clearing field had no significant effect on the error distribution, but that the errors increased when the time delay, T_D, was increased, e.g. with a time delay T_D = 1.6 μsec the standard deviation was ± 0.5 mm for the angular range 0 - 15°. Fukui and Miyamoto (1961) demonstrated that this lateral displacement of sparks is mainly due to the diffusion of primary electrons.

1.3g The Operation of Spark Chambers in Magnetic Fields

The operation of a spark chamber in a magnetic field has been of great interest and was successfully performed by Daion et al. (1960), Beall et al. (1960), O'Neill (1961), and Burleson et al. (1961).

Beall et al. (1960) applied a magnetic field, B, parallel to the plates and observed that, if a clearing field, E, was applied in the usual manner, sparks in alternate plates were displaced by amounts proportional to $\underline{E} \times \underline{B}$ in a direction parallel to the plates. For example with B = 13 kG, E = 80 v/cm, and time delay T_D = 1 μsec the relative displacement in successive gaps was about 1 cm.

The $\underline{E} \times \underline{B}$ displacement should increase the clearing times, since the electrons now move parallel to the plates and not normal to them, but Burleson et al. (1961) found clearing times of the order of 1 μsec for chamber fillings of helium and neon with and without alcohol additives.

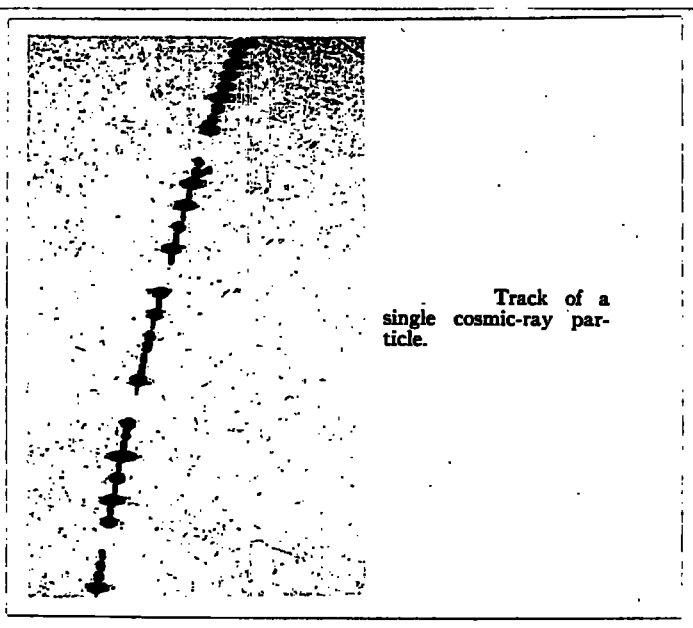

Track of a single cosmic-ray particle.

Figure 3.

Burleson et al. (1961) found that part of the $\underline{E} \times \underline{B}$ displacement was caused by the rising edge of the high voltage pulse, and the remainder by the D.C. clearing field. For 50% Helium and 50% Neon the lateral displacement varied between 0 and 2 mm with E = 250 volts/cm, B = 13k Gauss, and T_D = 0.20 μsec.

1.4 Applications of Spark Chambers

Spark chambers are well suited to measurements of the scattering of high energy particles, particularly if the particle flux is low and poorly defined in direction, because then conven-

tional counter equipment would yield very low counting rates.

Cork (1961), Cronin and Renninger (1960), and Cronin (1961) described experiments in which spark chambers with graphite or aluminium plates were used to measure proton polarisation by measuring left-right symmetries for protons which had been scattered in the plates of the chamber.

Where it ~~was~~ is not convenient to use the scattering material for the plates, as for instance in the case of liquid hydrogen, an external target may easily be used. Cork (1961) described some work on $K^+ + p \rightarrow K^+ + p$ and $\pi^- + p \rightarrow \pi^- + p$ scattering experiments, for which spark chambers were used to measure the directions. Several groups have constructed cylindrical spark chambers which have the advantage that the target can be completely surrounded by the chamber.

There are many experiments for measurements on scattering, polarization, particle decay or production, for which the spark chamber is the most useful detector.

In many applications the short recovery time and the short sensitive time make it possible to perform experiments which would be impracticable with alternative techniques.

Perhaps the most impressive demonstration of this is the Brookhaven neutrino experiment (Danby et al., 1962). For this a spark chamber of ten tons weight was constructed to observe the interactions of high energy neutrinos with matter. The important result which followed from this experiment was that there is a difference in the characteristics of the neutrinos resulting from π-μ and μ-e decay.

CHAPTER 2

Theoretical Considerations

2.1 The Discharge Mechanism

The physics of the development of a spark is very complicated and has been discussed in detail by a number of workers, notably Meek and Craggs (1953). The mechanism relevant to the development of a spark discharge under the conditions normally applicable to spark chamber operation is outlined below.

Consider a detector, consisting of two parallel plates a distance d cm apart in a gas at pressure p mm Hg, to contain a free electron near the cathode. A high electric field of E volts/cm is applied across the electrodes. If the ratio E/p is sufficiently large, the electron will ionise gas molecules during its acceleration towards the anode. The additional number of electrons created in this manner will also be accelerated in the applied electric field and cause further ionisation. When the original electron has moved a distance x towards the anode, the number of electrons created will be $\exp(\alpha x)$, where α is Townsend's first ionisation coefficient. This cumulative process is known as an electron avalanche. For neon the ratio of the masses of the positive ion and the electron is about 40.000:1 and therefore the ion may be considered stationary in comparison to the rapidly moving electrons. Consequently the avalanche develops across the gap as a cloud of electrons which leaves behind it the positive space charge, as shown in Fig. 4.a.

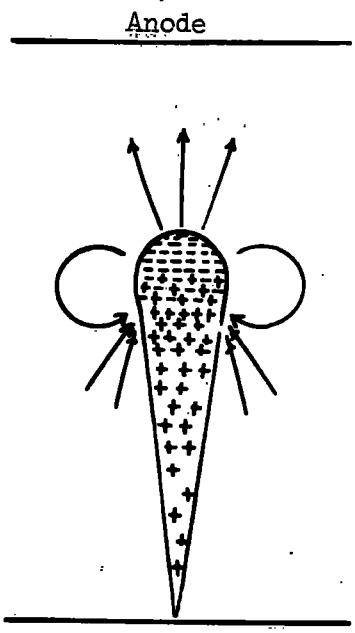

(a)

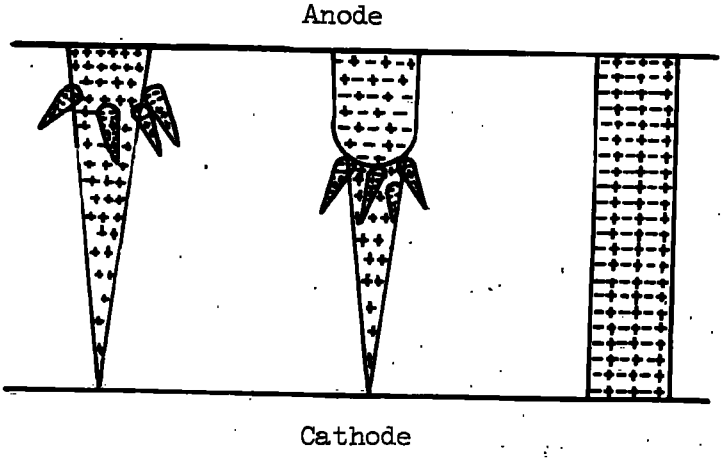

(b)

Figure 4 The Development of the Streamer

The space charge produced by the electron avalanche causes a distortion in the field across the gap, as shown in fig. 4.a. This distortion is greatest at the tip of the avalanche where the ion density is greatest. At this point the space charge field, E_r, supplements the externally applied field E as well as creating a field in a direction radial to the axis.

When the avalanche has crossed the gap, the electrons are swept into the anode and the slow positive ions remain in a cone shaped volume extending across the gap as illustrated in Fig. 4.b. the ion density is still comparatively low except at the anode and breakdown does not yet occur.

Photons are emitted from the densely ionised region in the avalanche and these produce photo-electrons in the gas surrounding the avalanche. The photo-electrons are thought to develop secondary avalanches. If the space charge field E_r is of the same order of magnitude as E, they will grow in a direction towards the stem of the main avalanche. The greatest multiplication of these secondary avalanches will occur along the axis of the main avalanche, where the space charge field E_r augments the external field E.

Positive ions left behind by these avalanches effectively extend the tip of the streamer and intensify the space charge of the main avalanche, which by this process advances towards the cathode as a self-propagating streamer. When it reaches the cathode a conducting filament of highly ionised gas is formed across the gap between the electrodes, and it is through this

filament that the external circuit discharges itself with a spark.

The transition from avalanche to streamer is considered to occur when the space charge field E_r is of the same order as the externally applied field E, because only in this case will the secondary avalanches be attracted towards the main avalanche. It should be noted that, since no secondary processes are involved, the characteristics of the spark are independent of the electrode materials.

The formative time of the spark in a uniform field consists mainly of the time taken by the avalanche to grow to the size where avalanche-streamer transition occurs: after this the streamer develops much more rapidly by photo-ionisation, so that its time of growth can be neglected compared to that of the avalanche.

The above analysis of spark formation was considered for only one initial electron. Ionising particles triggering spark chambers produce a number of electrons along their tracks and the above treatment must be slightly modified. This is most easily done by considering the mechanism of the slanting discharge.

2.2 The mechanism of the slanting discharge

Consider an ionising particle to have produced three electrons in the gap along its track, which makes an angle with the normal to the plates. Fig. 5a shows the growth of the corresponding electron avalanches initiated on application of the external electric field E. Fig. 5b shows the electric field distribution

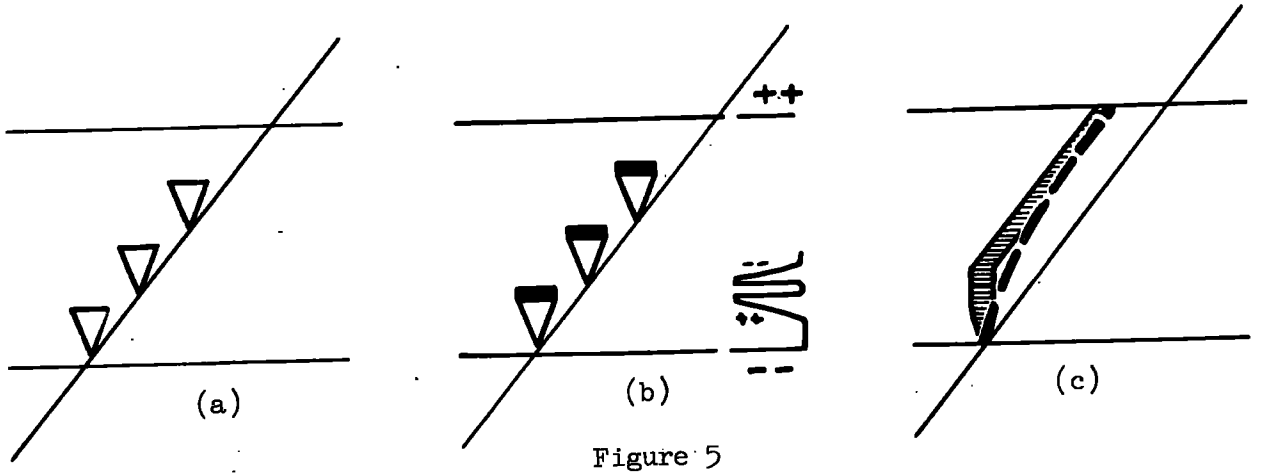

Figure 5

The Development of the slanting discharge

at a later time. It is proposed that when the space charge field E_r due to the positive ions is of the same order as the externally applied field E, the latter has been distorted to such an extent that the motion of any avalanche head is towards the nearest virtual anode, i.e. avalanche 1 develops towards avalanche 2. Such a model is easily extended to the case of 20 or so primary electrons. A consequence of this is that the sparks so produced should be concave with respect to the cathode, as illustrated in Fig. 5c, because of the finite distance the electron avalanches travel before the space charge fields are sufficiently strong. The model also predicts a maximum angle at which a spark can occur because as the trajectory of the primary particle becomes more oblique with respect to the external field direction, the avalanches will develop further apart and will eventually be too distant to interact with one another. Evidence for this is presented in Chapter 4.

2.3 The theoretical efficiency

The theoretical efficiency of a spark chamber is defined as the probability of a visible spark being produced when a selected ionising particle is followed by an applied high voltage pulse. The theoretical efficiency is suited to analysis and will be considered in detail below.

It is convenient to consider the mechanism of operation of a spark chamber in two parts. The first part concerns the time delay, T_D, which is the time interval from the passage of the triggering particle through the chamber to the instant of application of the high voltage pulse. The second part applies to the spark formation time, T_F.

During the time delay, T_D, the electrons and positive ions produced by the triggering particle diffuse. If a D.C. clearing field is applied they drift towards their respective electrodes. Electron attachment to electro-negative impurities in the noble gas in the chamber and the recombination of electrons with positive ions also play a small part.

During the spark formation time, T_F, only a fraction of the electrons removed by the above processes initiate electron avalanches, which finally culminate in the breakdown of the gap through a spark channel close to the original track of ionisation.

The two stages can be analysed quantitatively in a straightforward way and will now be considered in some detail.

Consider a detector consisting of two parallel plates a distance d cm apart in a noble gas at atmospheric pressure to have been traversed by an ionising particle which produced n_o free electrons in the gap. After the various processes by which electrons are lost in the time delay a mean number, n_1, of electrons remain. When the pulse is applied not all of the n_1 electrons will

be available to initiate electron avalanches, because a fraction of them will be attached during the pulse, leaving a number fn_1 remaining. Of these fn_1 a further fraction is swept to the positive electrode owing to the clearing done by the pulse itself. This will leave fn_2 electrons in the gap. It is assumed that the presence of any one of these in the gap at this stage is a necessary and sufficient condition for a spark. The probability of not one of the fn_2 electrons remaining is $\exp(-fn_2)$ i.e. the probability of obtaining a spark is then $1 - \exp(-fn_2)$, and since this is the definition of the efficiency, η, we may write

$$\eta = 1 - \exp(-fn_2) ;$$

the number, n_2, is derived below as a function of the operating conditions.

First, the number of electrons lost in the time delay, T_D, in applying the high voltage pulse is considered. The processes by which electrons are lost are: the clearing done by the D.C. clearing field, diffusion, recombination and electron attachment.

Clearing done by the clearing field

The effect of a static clearing field, E_c, is to drive electrons in the gap towards the positive electrode during the time delay T_D; n_c electrons will be captured by the electrode and thus removed from the gap. This number is given by

$$n_c = n_o \frac{\omega(E_c) \cdot T_D}{d}$$

where $\omega(E_c)$ is the drift velocity of an electron in the gas in

the field E_c.

Diffusion

The max. value of T_D which was normally used was $T_D = 2.5$ μsec. It is shown in Chapter 4 that the number of electrons lost in this time by diffusion to the electrodes is negligibly small compared with the clearing done by the clearing field. The diffusion loss is therefore neglected.

Recombination

The rate of loss of electrons due to recombination with positive ions is given by

$$\frac{dn}{dt} = -\alpha_i n^2$$

where n is the ion concentration per unit volume and α_i is the recombination coefficient, given by $\alpha_i = 2.1 \times 10^{-7}$ (ions/cc.sec)$^{-1}$ for neon. For an initial number of ion pairs, n = 20, the number, n_R, of electrons lost due to recombination in 10 μsecs will be given by

$$n_R = \frac{2.1 \times 10^{-7} \times 20^2 \times 10^{-5}}{8.4 \times 10^{-10}}$$

A complication arises in this calculation because of the relatively dense ionisation produced along the track of the ionising particle. This gives rise to an initial spatial distribution of ionisation which is far from uniform. Since the recombination loss rate is dependent on the square of the ion density, which is high along the track of the ionising particle, one would expect a high

apparent value of α_i which would become lower when the ion density had become uniform over say, one c.c. Sayers (1938) calculated an apparent change in α of only about one order of magnitude, and consequently the recombination loss may also be safely ignored.

Attachment

It will be shown in Chapter 4, where results of electron attachment to impure gas mixtures are presented, that for the present case of low contamination, the electron attachment during the time delay, T_D, may be neglected.

After a time delay, T_D, of not greater than about 2.5 μsecs the only appreciable electron loss is due to the clearing field, leaving a mean number, n_1, of electrons given by

$$n_1 = n_o - n_c$$

The instant of application of the high voltage pulse marks the beginning of two further processes of electron loss.

One of these is electron attachment to impurities in the gas. These largely consist of oxygen which has a high attachment cross-section for electrons of energy 2 eV and alcohol vapour where this is a constituent. It is thought that as the electrons accelerated by the high voltage pulse reach energies approaching 2 eV, they incur the risk of attachment to oxygen impurities and this is equivalent to a number, fn_1, of the n_1 electrons in the gap immediately before the onset of the high voltage pulse.

After this, a further fraction, g, of these remaining electrons will be swept out of the gap. The value of g depends on the relative magnitudes and directions of the clearing field and the high voltage pulse. The two relative field directions will be considered in turn.

(a) Fields in the same direction

In this case the fraction, g, of the fn_1 electrons in the gap, which are captured by one of the electrodes, is given by

$$g = \frac{\int_0^{T_F} \omega\{E(t)\}dt}{d}$$

where $\omega\{E(t)\}$ is the drift velocity of the electrons in the gas in the field E(t). Thus the total number of electrons, which are capable of initiating avalanches, finally remaining in the gap is

$$fn_2 = fn_1(1-g)$$
$$= fn_o\left\{1 - \frac{\bar{\omega}(\bar{E}_c)\cdot T_D}{d}\right\}\left\{1 - \frac{\int_0^{T_F} \omega\{E(t)\}dt}{d}\right\}$$

(b) Fields in opposite directions

Two cases must be distinguished, depending on the relative magnitudes of the clearing done by the D.C. clearing field and the high voltage pulse. If the fraction, n_c/n_o, of the clearing done by the clearing field is greater than the fraction, g, of the clearing done by the high voltage pulse, the number of electrons cleared out of the gap remains numerically equal to n_c. Alternatively, if $g > n_c/n_o$, the number of electrons cleared out of the gap depends only on g.

Setting $n_o = \nu d$, where ν is the specific ionisation of the triggering particles in the gas of the chamber, the following expressions for the theoretical efficiency are obtained.

(a) Fields in the same direction:-

$$\eta = 1 - \exp\left[-f\nu d\left(1 - \frac{\bar{\omega}(E_c)T_D}{d}\right)\left(1 - \frac{\int_o^{T_F} \omega\{E(t)\}dt}{d}\right)\right] \quad \ldots\ 1.$$

(b) Fields in the opposite direction:-

$$\frac{n_c}{n_o} > g \qquad \eta = 1 - \exp\left[-f\nu d\left\{1 - \frac{\bar{\omega}(E_c)\cdot T_D}{d}\right\}\right] \quad \ldots\ 2.$$

$$\frac{n_c}{n_o} < g \qquad \eta = 1 - \exp\left[-f\nu d\left\{1 - \frac{\int_o^{T_F} \omega\{E(t)\}dt}{d}\right\}\right] \quad \ldots\ 3.$$

Here it should be pointed out that equation 1. differs from that obtained by Burnham et al. (1963) because they erroneously assumed that the number of electrons cleared out of the gap by the high voltage pulse was gfn_o and not $gf(n_o - n_c)$. However, the expression was not used by Burnham et al. (1963) in their analysis of the experimental data and therefore did not invalidate their conclusions.

There are several ways of applying these theoretical expressions to an analysis of the experimental data. The method adopted in this thesis is to use the equations 1., 2. and 3. together with the measured variation of efficiency with clearing field and high voltage pulse characteristics to derive the value of f and to determine the electron mobility and drift velocity for a variety of fields. A

check on the validity of the suggested mechanism is then effected by an examination of the consistency of the values of f so obtained.

CHAPTER III

The Experimental Arrangement

3.1 The Spark Chamber

In the investigations a spark chamber containing six parallel plate spark counters was used. The spark counters were constructed of 14 gauge aluminium and arranged one above another. The dimensions of the cathode plates were 4.3 x 18.5 cm^2, and the dimensions of the anode plates were 9 x 16.5 cm^2. These yielded a sensitive area of 4.3 x 16.5 cm^2. The gap width was 1 cm. All the edges of the plates were rounded to avoid spurious breakdown. The plates were washed with acetone and water and polished with muslin. Each counter comprised an individual unit mounted on a perspex base, the lower plate being attached to the perspex base by four countersunk bolts. The upper plate of the unit was supported above the perspex base by four $\frac{3}{4}$" 8BA brass bolts, which were used to adjust the plate separation of each counter to 1 cm with an accuracy of $\pm\frac{1}{2}\%$.

The complete unit, comprising six such spark counters arranged vertically above one another, was contained inside a cylindrical vessel of diameter 27.5 cm and depth 12.5 cm. The back of the cylinder was constructed of $\frac{1}{4}$" thick brass. The high voltage pulse applied to the plates was fed to the chamber via commercial spark plugs, which were screwed tightly into the brass plate to make a vacuum seal. The cylinder walls were made of Pyrex glass $^5/_{32}$" thick,

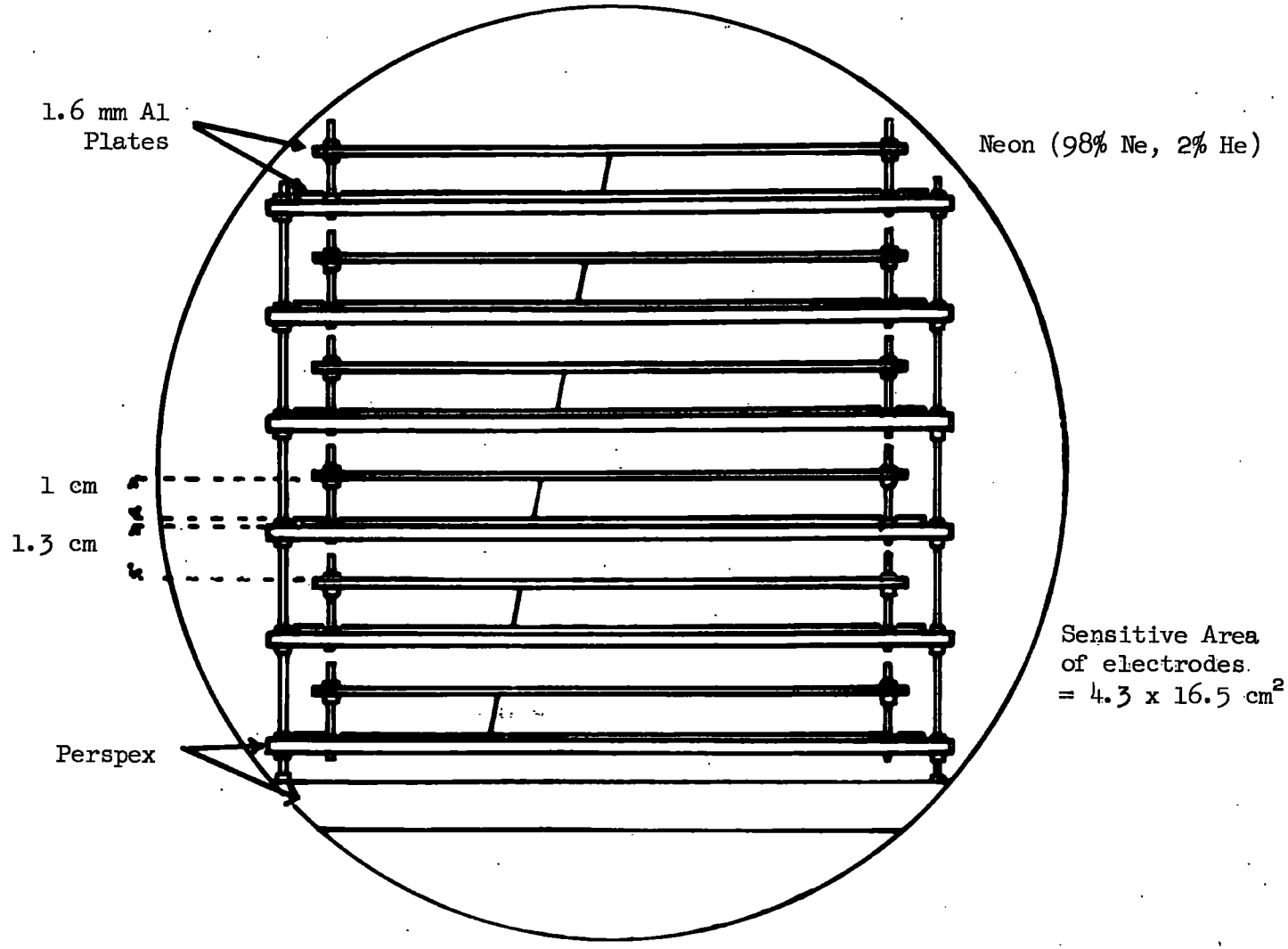

Figure 6 The Spark Chamber

and the front plate was a disc of $\frac{1}{4}$" thick armour-plate glass. The whole was held together by four long bolts running the length of the cylinder. A vacuum seal was maintained by means of rubber gaskets and Apiezon grease.

The cylinder was evacuated using a rotary pump only and refilled via a liquid air trap with B.O.C. commercial neon to a pressure of 1.1 atmospheres.

TABLE 2

Constituents of B.O.C. commercial neon

Gas	Concentration (%)
Neon	98 ± 0.2
Helium	2 ± 0.2
Oxygen	10^{-3}
Nitrogen	10^{-2}
Argon	5×10^{-5}

The estimated oxygen content of the chamber gas after filling, by comparison with standard calibrated neon discharge tubes, was of the order of 10^{-2}%.

Due to the fact that the counters were photographed from a distance of 112 cm, the individual counter units were arranged fan-wise to the axis of the camera lens, so that their central planes passed through the camera lens. As a result of this fanning arrange-

ment, which ensured that as much of each gap as possible was visible to the camera lens, an insensitive gap of varying width was created between adjacent counters. The spacing of this gap was adjusted to be at least 1.3 cm. Fig. 6 shows the arrangement as it appeared to the camera lens.

The plates of the counter were connected directly in parallel so that in each counter the lower plate was the cathode and the upper plate was the anode.

3.2 The Electronics

The electronic circuits which were employed in the operation of this spark chamber may conveniently be divided into two parts:- a) the event selection system, and b), the high voltage pulse generator.

3.2a The Event Selection System

The spark chamber was triggered by cosmic ray particles. These were detected by two identical scintillation counters of area 2.5 x 15 cm^2 placed directly above and below the assembly of counters. An E.M.I. Type 9524S photomultiplier was coupled to each scintillation counter. Each photomultiplier output pulse was fed through a discriminator to a coincidence circuit and then to a variable delay line. The coincidence rate was 0.8/min. Although the details of these circuits are not considered here, it is emphasised that their design was such as to minimise the time delay between the passage of a charged cosmic ray particle through the two scintillation counters and the appearance of the pulse which triggered the high voltage pulse generator. Fig. 7

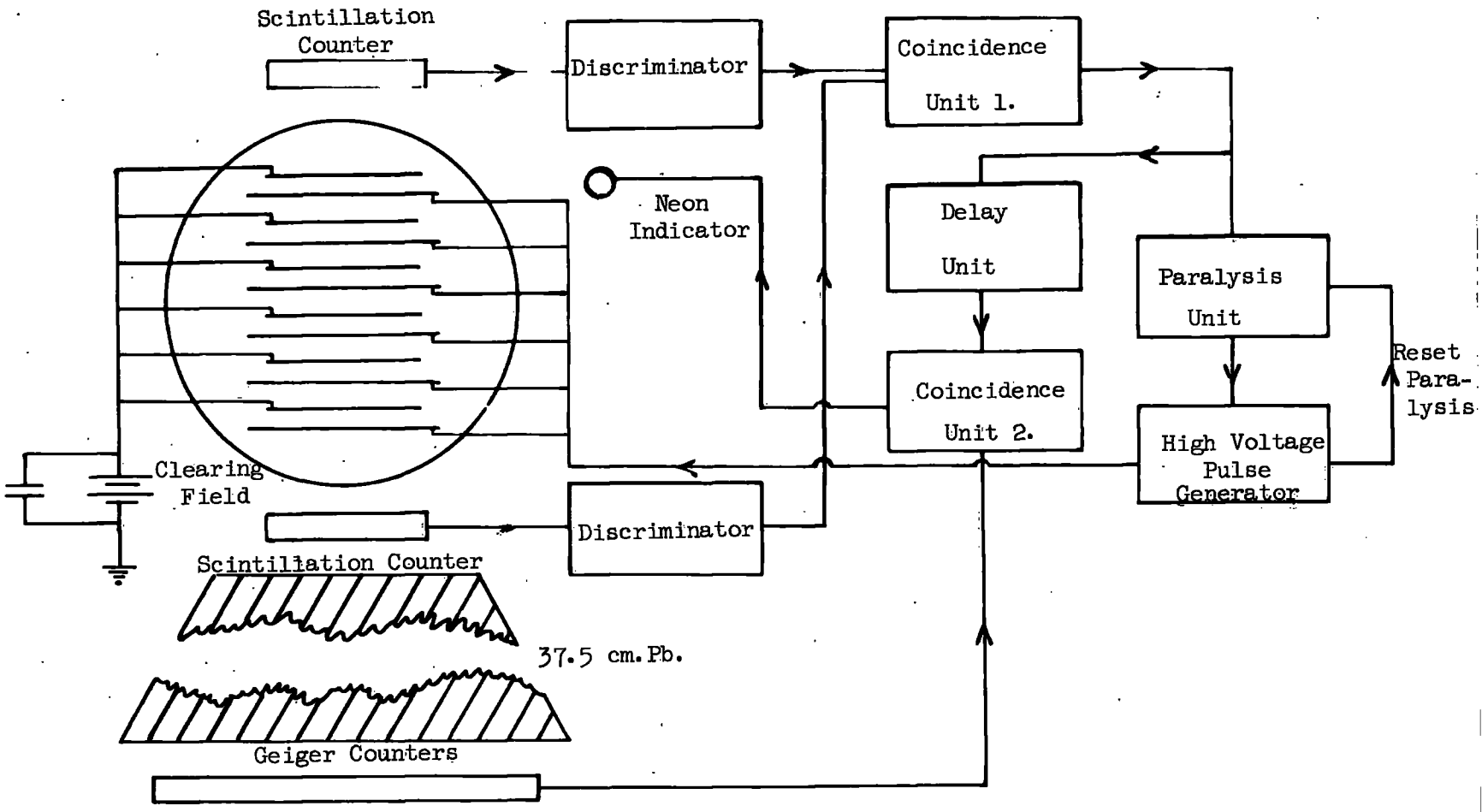

Figure 7. Schematic Diagram of the Apparatus

shows a block diagram of the electronic circuits.

A coarse division between particles of high and low energy was afforded by 37.5 cm of lead and a tray of Geiger counters beneath the scintillation counters. A particle which had traversed both scintillation counters and the lead initiated a third pulse in one of the Geiger counters. This pulse was fed to a second coincidence circuit which caused a small neon indicator bulb beside the chamber to be lit whenever the pulse from the Geiger counter and the coincident pulse from the two scintillation counters were received within 5 μsec. The sparks were recorded photographically and subsequent examination of the film indicated which trajectories were due to high energy particles. (The minimum energy required by a muon to penetrate the lead was 500 MeV).

This arrangement was used to select energetic particles for measurements of the accuracy of track location so that the effects of scattering in the aluminium plates of the chamber should be negligible.

3.2b The High Voltage Pulse Generator

The output pulse from the variable delay line was fed to the grid of an EFP 60 secondary emission valve. This supplied a triggering pulse of amplitude 200V to a large hydrogen thyratron (Mullard XH16). This in turn discharged a condenser, charged to several kilovolts, through a resistance in parallel with the chamber. This

circuit, which defined all the constants of the pulse, and is shown in Fig. 8.

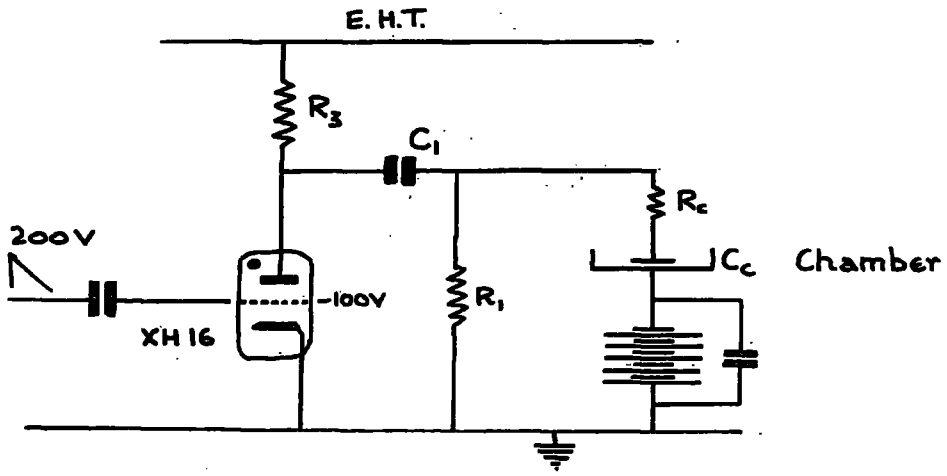

Fig. 8 The pulse generator circuit.

The decay time of the pulse is governed by the product C_1R_1; for typical operation of the chamber the pulse decayed with a time constant of 0.1 μsec (R_1 = 100Ω, C_1 = 1000 pF). The rise time of the pulse across the chamber depends on the product R_cC_c; a typical value was 50 nsec as measured on a Tektronix 543 oscilloscope with a P6014 high voltage probe.

The minimum time delay in the arrival of the high voltage pulse at the spark chamber after the traversal of the triggering cosmic ray particle was 0.45 μsec. Provision was made for the application of a steady D.C. clearing field across the spark chamber, and this was derived from a 120V dry battery.

The sparks were recorded photographically on Ilford HPS 35 mm film at an aperture of f3.5. The camera had an open shutter and the electronic circuitry was paralysed after each event for the winding period of the camera. This was set to be approximately 10 secs, more than ample to allow the condenser C_1 to be recharged through R_s (60 MΩ), and the E.H.T. supply to recover. This was capable of delivering a few milliamps at a variable voltage up to 15 kV.

CHAPTER IV

The experimental results

The experimental results are presented in three sections appertaining to the efficiency, the geometrical properties of the sparks, and the effect of impurities. In what follows the gas filling was a mixture of neon and alcohol (1.1 atmospheres neon, 4.4 cm alcohol) unless otherwise stated.

4.1 The efficiency results

4.1a The spark formation time

In order to solve the equations (1), (2) and (3) (quoted on page 25) it is necessary to know the approximate values of T_F, the spark formation time. When the high voltage pulse is applied to the plates immediately after the passage of an ionising particle, the voltage pulse collapses very rapidly after a certain time, presumably at the instant the spark occurs. The time from the beginning of the pulse to the onset of the rapid collapse of the pulse is T_F. This was measured by displaying the pulse applied to the plates after the passage of an ionising particle on a Tektronix 543 oscilloscope and recording the image photographically on Ilford 5G91 film. Approximately 200 superposed pulses were required to obtain a satisfactory record. Fig. 9 is a typical photograph obtained in this way (Pulse height = 4 kV, T_F = 280 nsec, T_R = 27 nsec, T_{decay} = 800 nsec).

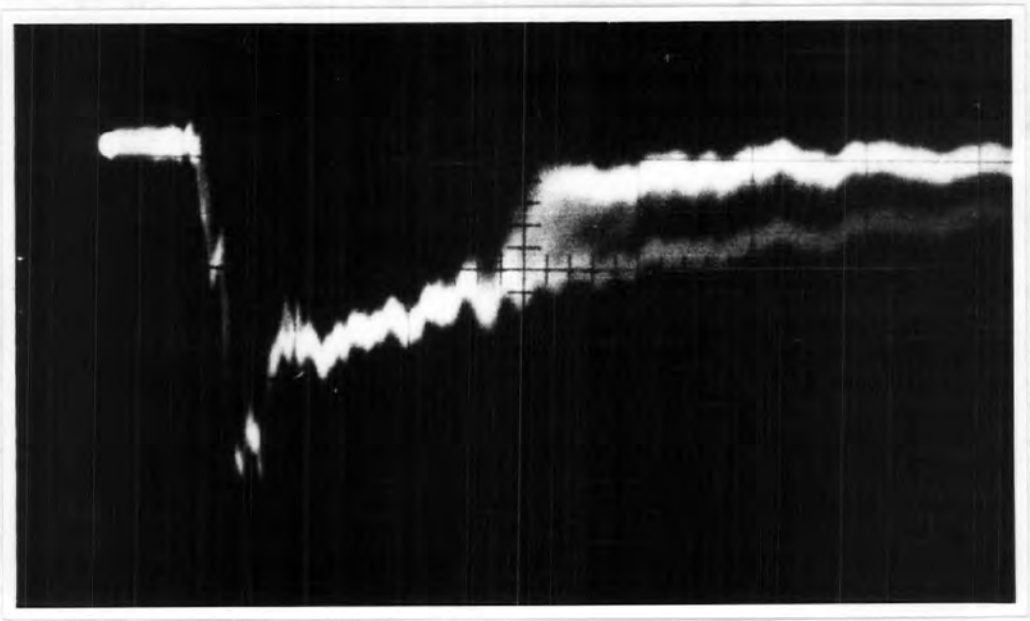

Fig. 9. Breakdown of the high voltage pulse

T_F was investigated as a function of the applied high voltage pulse for different rise and decay times. The results are plotted in Fig. 10 (the rise and decay times are defined in Fig. 11), which shows that there is a very rapid decrease in T_F with increasing pulse height, and, to a lesser degree, with increasing pulse decay time. Such a reduction is expected in view of the increase of Townsend's ionisation coefficient and of the electron mobility with increasing electric field.

The results of Fischer and Zorn (1961), who investigated the effect of alcohol on the formative times in argon and helium, indicate that the formative time in a noble gas-alcohol mixture may differ greatly from that in the noble gas alone. Consequently,

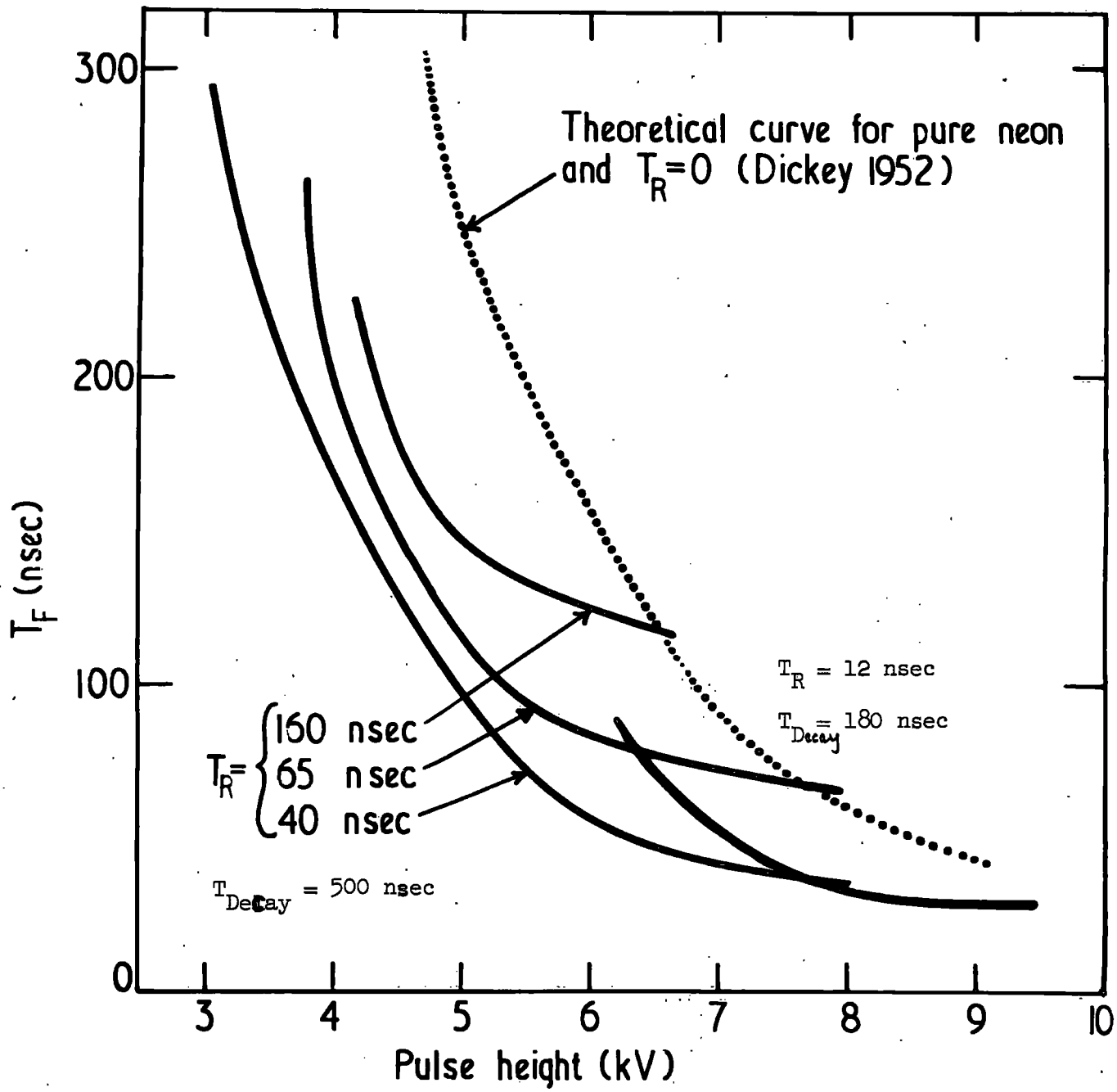

Fig. 10 Spark formation times as a function of the height of the applied pulse

and also in view of the relatively impure nature of the neon used in these experiments, a direct comparison of the results of this work with those of other workers would not be very meaningful. Suffice it to say that the values presented in Fig. 10 are close to those for neon alone obtained by Fischer and Zorn.

The variation in T_F from one spark to another was found to be less than 10% of the mean (see Fig. 9). Although an accurate estimate of the rate of collapse of the voltage due to a spark taking place could not be made, the mean rate of collapse appears to be about 3×10^{11} volts/sec.

4.1b The variation of the efficiency with the parameters of the pulse

Observations on the variation of efficiency with applied voltage show that the striking potential for a 1 cm gap is 3.5 ± 0.5 kV for long pulses. In the present case of a multi-gap spark chamber the efficiency refers to the probability per gap of a spark being formed. The voltage characteristics are shown in Fig. 11, from which it may be seen that the striking potential is dependent on the decay time of the pulse and to a lesser extent upon the rise time.

For a given pulse height it is evident that the efficiency decreases with increasing rise time and decreasing decay time. For pulses with fast rise times the efficiency of the chamber is

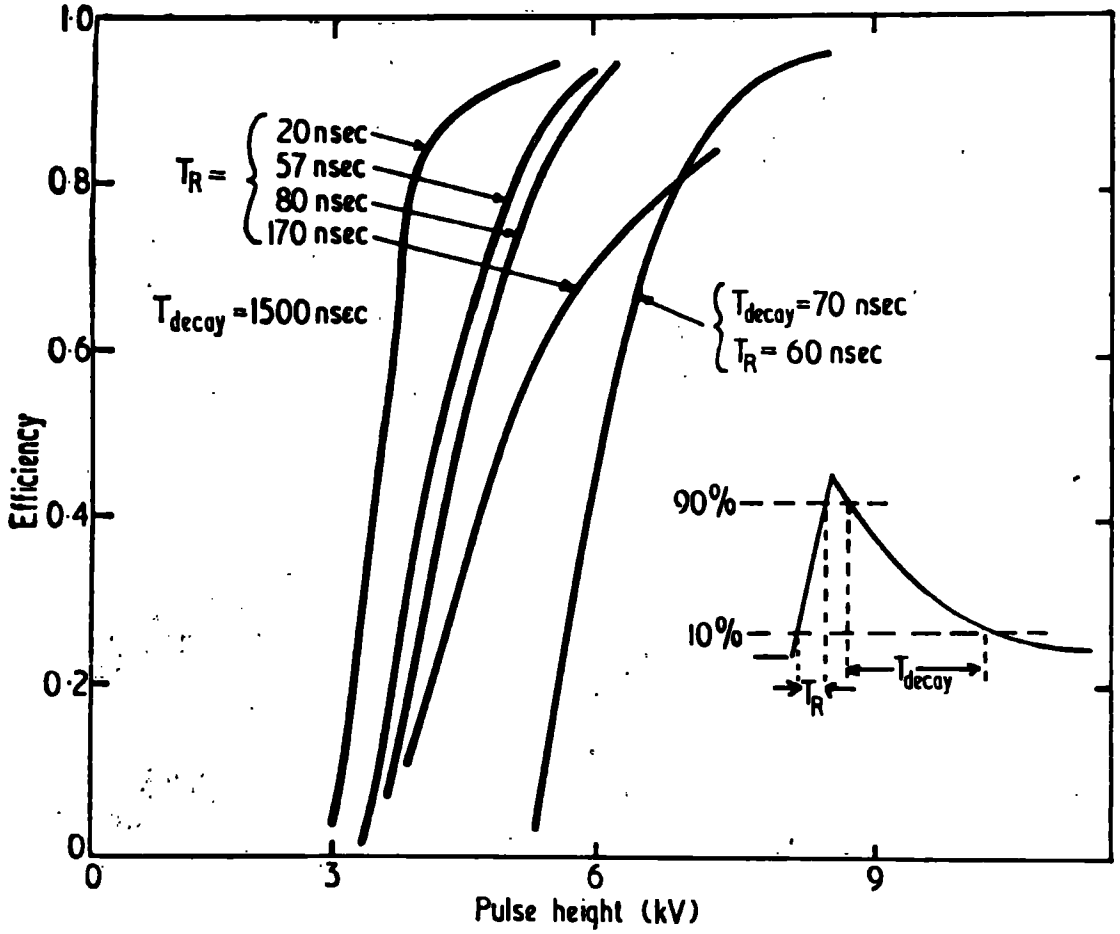

Figure 11 The efficiency as a function of the height of the applied pulse.

about 90% at 5 kV pulse height and 98% above 7 kV. There is a useful working region of several kilovolts throughout which the efficiency is greater than 90%, the upper limit of the voltage (12 kV) being set by the onset of spurious sparks.

The data given in Fig. 11 can be used to derive the mean electron mobility over the range of high voltage fields used. The mean mobility of the electrons in the neon-alcohol mixture is defined by

$$\overline{K[E(T_F)]} = \frac{\int_0^{T_F} K[E(t)]E(t)dt}{\int_0^{T_F} E(t)dt}$$

For the case of zero clearing field equation (1) can be written as:

$$-\ln(1-\eta) = f\nu d\left\{1 - \frac{\int_0^{T_F} \omega[E(t)]dt}{d}\right\}$$

$$\text{i.e.} \quad \ln(1-\eta) = -f\nu d\left\{1 - \overline{K[E(T_F)]}\frac{\int_0^{T_F} E(t)dt}{d}\right\}$$

Fig. 12 shows $\ln(1-\eta)$ plotted against $\int_0^{T_F} E(t)dt$ for a pulse of rise time 40 nsec. The measured values lie close to a straight line as expected. Assuming $\nu = 20$, a least squares fit for the slope and the intercept yields the values $f = 0.24 \pm 0.02$ and $\overline{K[E(T_F)]} = (1.6 \pm 0.2) \times 10^3 cm^2 sec^{-1} v^{-1}$ over the range of applied voltage.

These results are given in Table 3, together with values of f and $\overline{K[E(T_F)]}$ calculated in a similar manner for pulses of different rise times.

Fig. 12 The ineffeciency $(1-\eta)$ as a function of

$$\int_0^{T_F} E(t)dt$$

$(T_R = 40$ nsec$)$

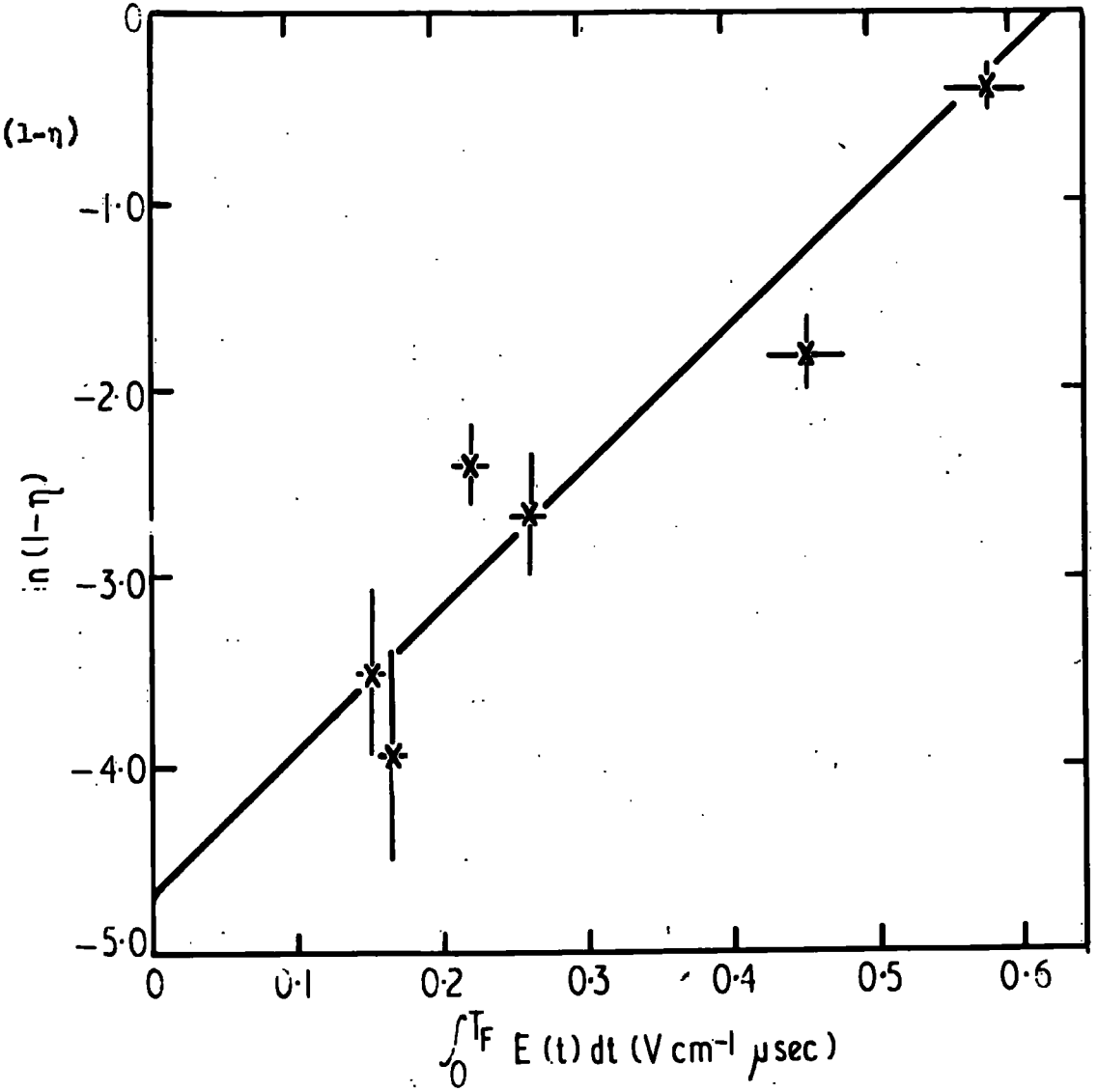

Table 3

Variation of f and $K[E(T_F)]$ with pulse rise time

pulse rise time (nsec)	f	$K[E(T_F)]$, x 10^3 ($cm^2 sec^{-1} v^{-1}$)
40	0.24 ± 0.02	1.6 ± 0.2
80	0.28 ± 0.02	2.5 ± 0.3
170	0.28 ± 0.02	3.4 ± 0.4

In addition to determining the overall mean electron mobility, the mean electron velocity has been found for each point in Fig. 12. The lack of constancy of the mobility with respect to the electric field makes it necessary to specify an average field to which the value refers. This average is taken to be the value E_o such that $E_o = (1/T_F)\int_o^{T_F} E(t)dt$. The mean electron velocity is then given by

$$\omega(E_o) = (1/T_F)\int_o^{T_F} \omega[E(t)]dt$$

and follows directly from the application of equation (1). The values are given in Fig. 19, where data for two other values of T_F (80 and 170 nsec) are included.

At this stage it is relevant to point out that the fact that the variation shown in Fig. 12 is linear suggests that the factor f (§2.3) is sufficiently constant independent of pulse height for the purposes of the present analysis.

Fig. 13 shows the efficiency of the chamber as a function of the pulse rise time for a 6 kV pulse. The rise time of the pulse was varied both by increasing the capacity of the chamber and by varying the resistance in series with the chamber, both methods giving similar results. Assuming that the variation of efficiency with rise time is due to the variation of the clearing done by the pulse with varying rise time, the variation can be compared with the theoretically predicted values based on the measured spark formation times.

Since the spark formation time has been measured for pulses of only three different rise times, the comparison between the experimental and theoretical values is somewhat limited. However, the three points predicted theoretically are in good agreement with the experimental points, thus varifying the basic principles of the theory.

4.1c The efficiency as a function of the time delay

The measurements described here have been made using a 6 kV pulse with a rise time of 40 nsec and a decay time of 300 nsec. With no clearing field the efficiency as a function of time delay is 90% at 7 μsec, 50% at 11 μsec, and 10% at 15 μsec. This rate of decrease is similar to that reported by Fukui and Miyamoto (1961), and is ascribed by them to the loss of the initial electrons by diffusion to the electrodes.

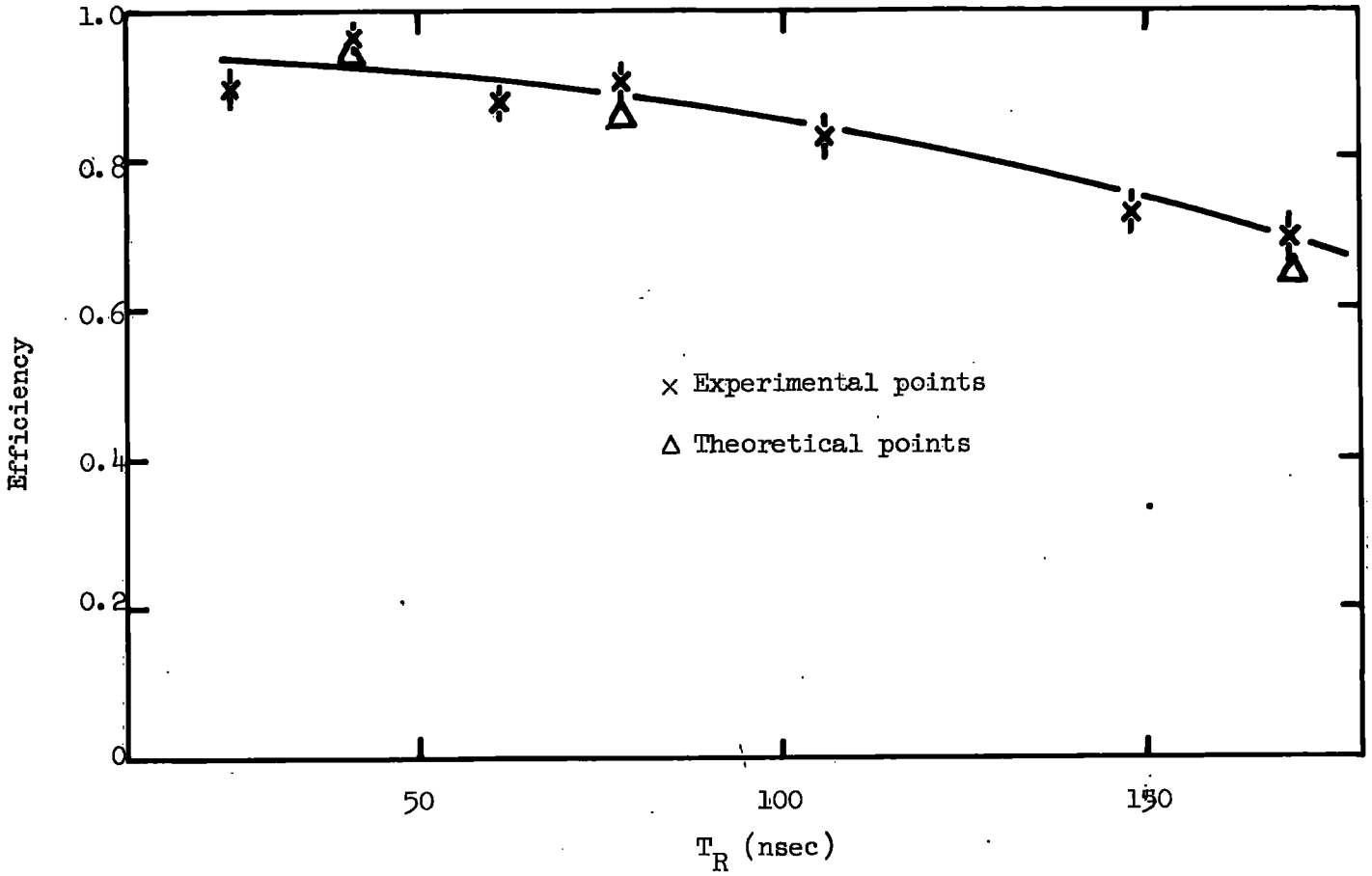

Fig. 13 The efficiency of the chamber as a function of the pulse rise time for a 6 kv pulse

Figures 14 and 15 show the efficiency curves as a function of time delay for various clearing fields applied in the two relative field directions. Although the minimum time delay in applying the high voltage pulse to the plates was 0.45 μsec, clearing fields of up to 1000 v/cm were applied in an attempt to show the presence of a minimum in the curve of sensitive time against clearing field, the sensitive time being defined as the time for the efficiency of the gap to fall to 50% as suggested by Roberts (1961). No sparks were produced for clearing fields in the range 240 v/cm to 1000 v/cm and no minimum in the sensitive time was found. This is in disagreement with the results of Cronin and Renninger (1960) who found a minimum at E_c = 140 v for a gap of width 0.95 cm.

For a constant clearing field the sensitive time is smaller when the field is in the same direction as the pulse than when the field is in the opposite direction to the pulse. This is consistent with the suggested mechanism, in which it is proposed that some electrons are cleared out of the gap by the pulse itself before the discharge occurs.

When the clearing field is in opposition to the pulse, and the efficiency is low, it can be assumed that the clearing done by the pulse is negligible compared with that done by the clearing field. Under such conditions the value of the time delay for which the efficiency tends to zero, T_{DO}, is closely related to the mobility of the electrons in the neon-alcohol mixture. The values

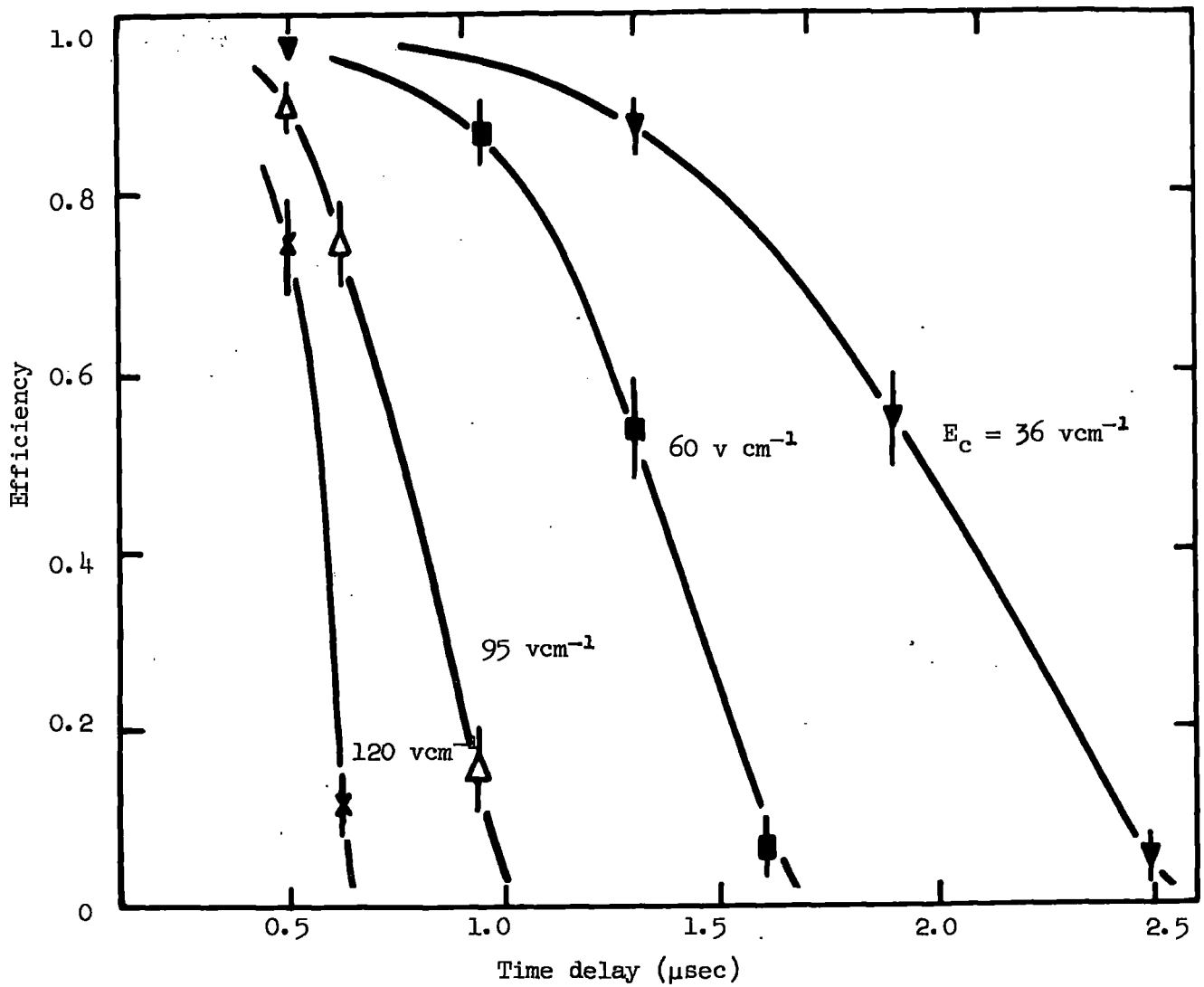

Fig. 14 The efficiency as a function of T_D for the case of the clearing field (E_c) in the same direction as the pulse field.

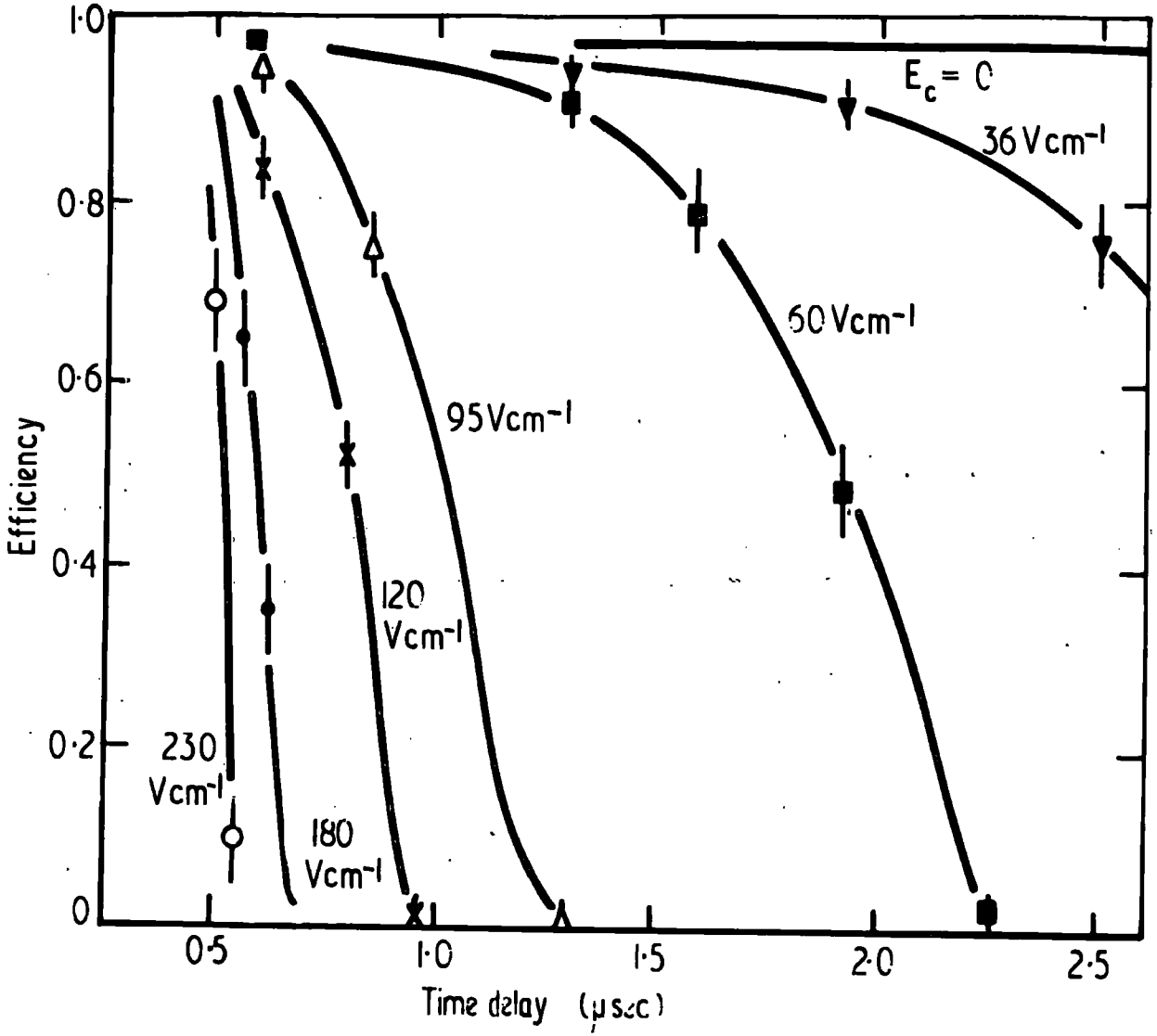

Fig. 15 The efficiency as a function of T_D for the case of the clearing field (E_c) in the opposite direction to the pulse field.

of T_{DO} are plotted against the reciprocal of the appropriate clearing field in Fig. 16. Defining $\overline{K(E_c)} = \omega(E_c)/E_c$ equation (2) yields the relation

$$1 - \frac{\omega(E_c)T_{DO}}{d} = 0$$

$$\text{i.e.} \qquad T_{DO} = \frac{1}{\overline{K(E_c)}} \propto \frac{1}{E_c}.$$

The slope of the line is therefore equal to $\overline{K(E_c)}^{-1}$ from which $\overline{K(E_c)}$ is found to be $7.8 \times 10^3 cm^2 sec^{-1} v^{-1}$ for a range of E/P from 0.05 to 0.33 v $cm^{-1}(mmHg)^{-1}$. The electron velocities corresponding to each of the points in Fig. 16 are shown in Fig. 19.

It is possible to combine the results to give a universal curve of efficiency against the product of the time delay and the clearing field. The curves for the two cases of relative field direction are shown in Figs. 17 and 18.

When the clearing field is acting in the opposite direction to the pulsed field, and the fraction of the clearing done by the former is greater than the fraction done by the latter, equation (2) may be written as

$$\ell n(1-\eta) = -f\nu d + f\nu\omega(E_c)T_D$$

Applying the method of least squares to a plot of $\ell n(1-\eta)$ against $E_c T_D$ yields f = 0.27 and $K(E_c) = 8 \times 10^3 cm^2 sec^{-1} v^{-1}$ in good agreement with the results for f (table 3) and $\overline{K(E_c)}$ (above) already obtained.

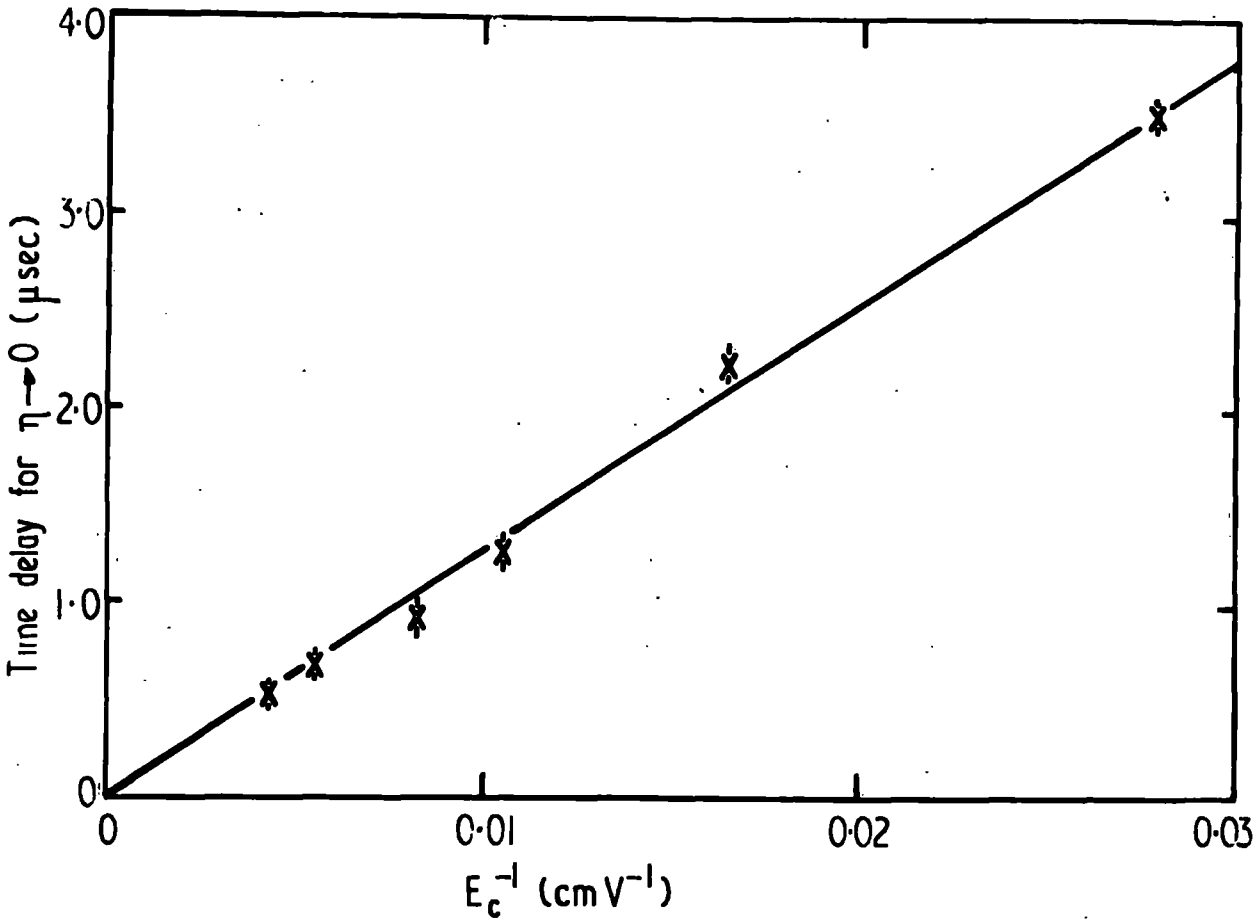

Fig. 16 The time delay (T_{DO}) in which the efficiency falls to zero as a function of E_c^{-1} for E_c in opposition to the pulse field. (T_R = 4.0 nsec, pulse height = 6 kV).

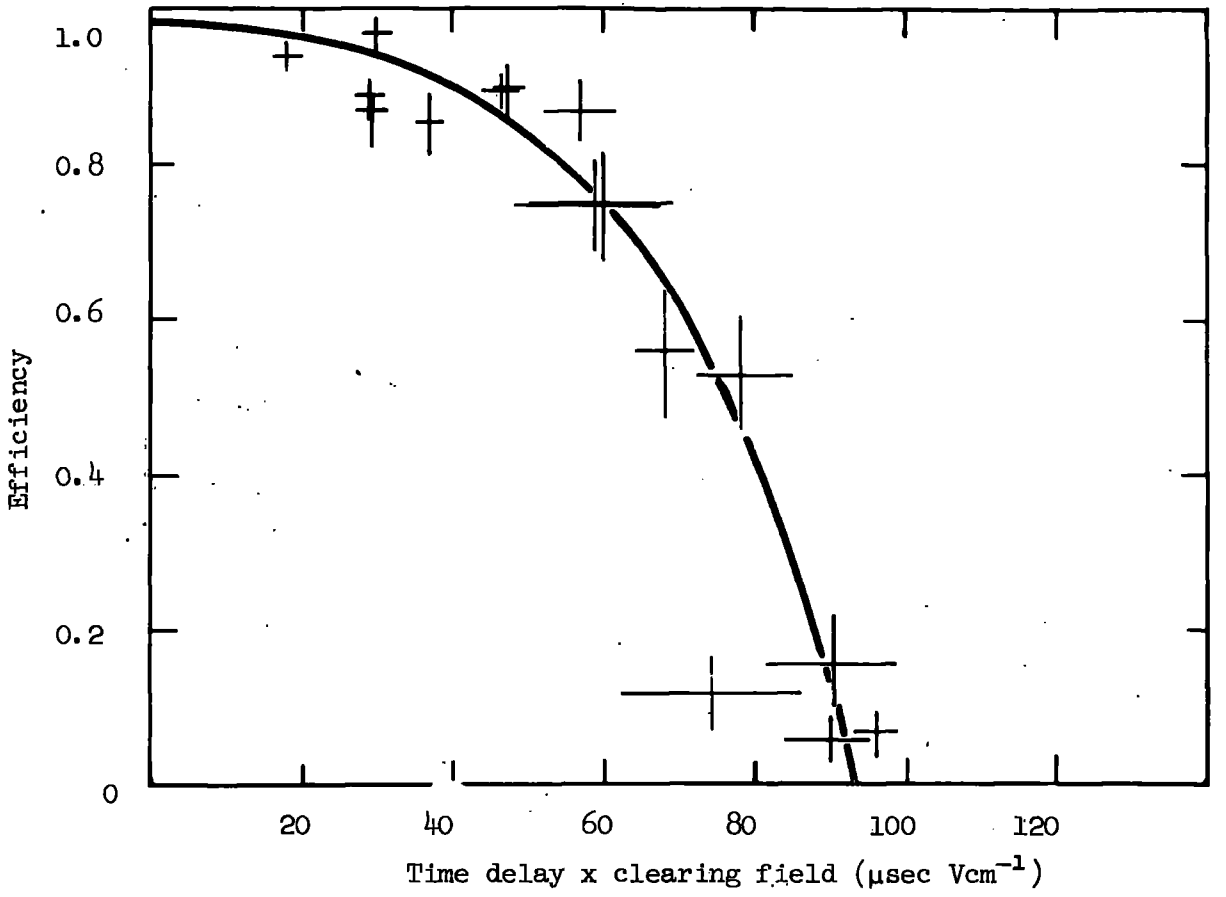

Fig. 17 Universal relation between efficiency and the product of T_D and E_c for E_c in the same direction as the pulse field.

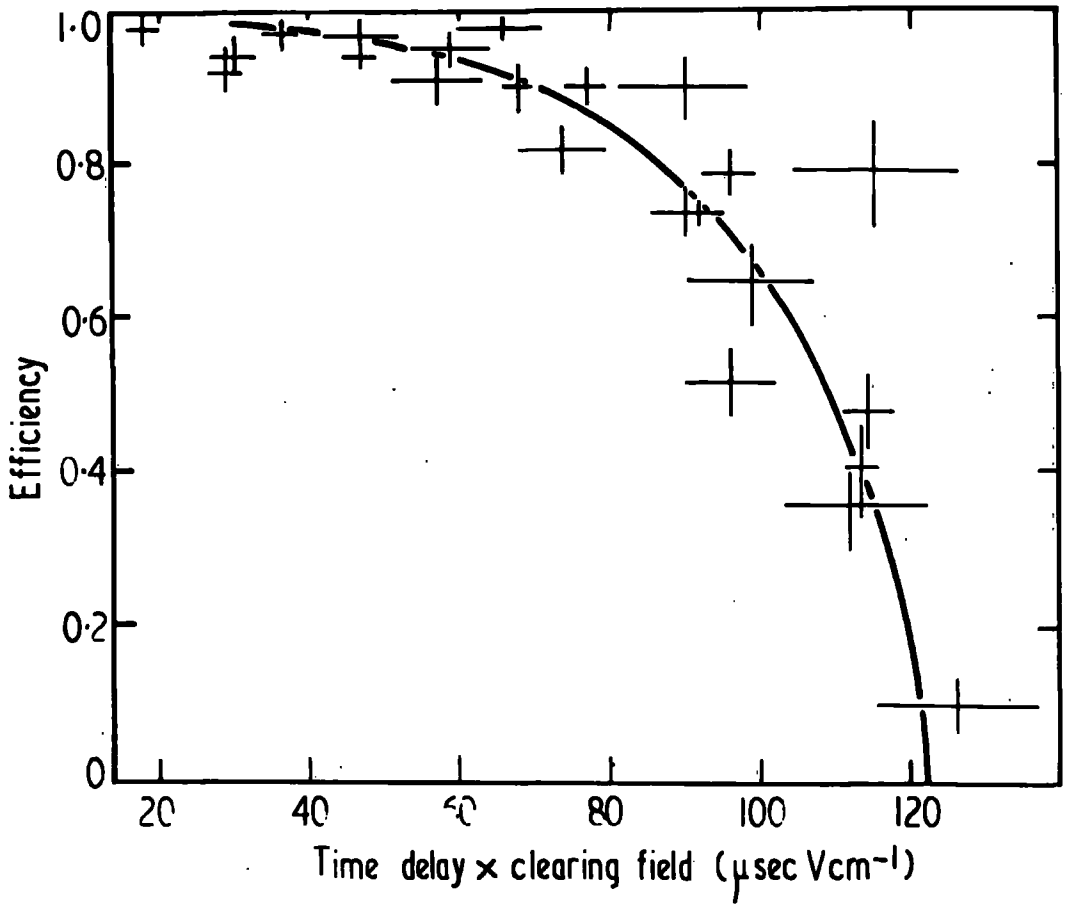

Fig. 18. Universal relation between efficiency and the product of T_D and E_c for E_C in opposition to the pulse field.

From the results for the case of the clearing field in the same direction as the pulse field a value of 0.30 ± 0.05 cm is found for the clearing done by the 6 kV pulse before it reaches its critical potential, corresponding to a mean value of $K[E(T_F)]$ of $(1.6 \pm 0.3) \times 10^3 cm^2 sec^{-1} v^{-1}$ over the range of applied voltage (cf. the values of $K[E(T_F)]$ given in table 3).

The efficiency of the chamber as a function of time delay for no clearing field was measured with a similar pulse, but of pulse height 8.5 kV. This showed that at a particular time delay an appreciable increase in efficiency may be obtained by increasing the pulse height. A not unreasonable explanation for this is that the corresponding decrease in T_F (see fig. 10) will reduce the clearing done by the pulse, so causing a subsequent increase in efficiency.

4.1d Discussion of the efficiency results

The results show that the electron mobility falls considerably in going from the values of E/P relevant to the usual clearing fields ($\tilde{<}0.33$ $vcm^{-1}(mm\ Hg)^{-1}$) to those for the applied pulse ($\tilde{<}8$ $vcm^{-1}(mm\ Hg)^{-1}$). Some variation in the mobility with rise time has been found which would appear to indicate an inconsistency in the model, but a partial explanation is advanced later.

In view of the variation of mobility with E/P it is easier to compare the results with more direct measurements by examining the values found for the electron drift velocity. The velocities

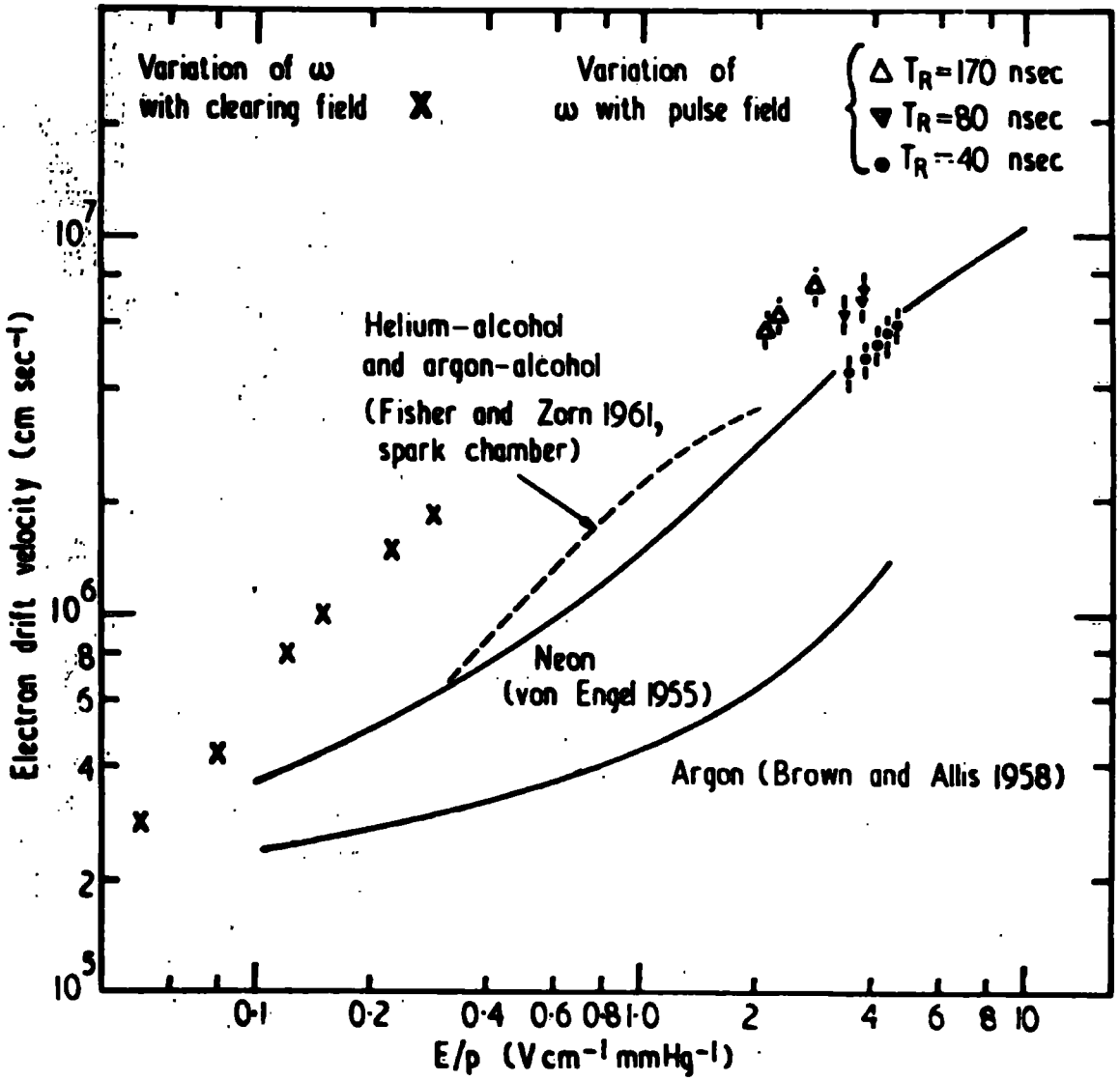

Figure 19 Drift velocities of electrons as a function of *E/p*. The points refer to the results of the present experiment.

derived from the present experiments for the neon-alcohol mixture are shown in Fig. 19. These may be compared with the variation given by von Engel (1955) for pure neon also shown in the figure. The higher velocities in the mixture, which are particularly marked at low values of E/P, are attributed to the effect of alcohol. Support for this suggestion comes from experiments by other workers; thus, the drift velocities in an argon-alcohol mixture calculated from the results of Fischer and Zorn (1961) are seen to be considerably higher than those found for pure argon by Nielsen (1936, reported by Brown and Allis, 1958). It must be pointed out, however, that the recent results of Beall et al. (1960), for argon alone, indicate a drift velocity much greater than that found by Nielsen and greater even than the velocities found by Fischer and Zorn. The grade of argon used by Beall et al. and by Fischer and Zorn, namely "welders grade argon", was the same. A possible explanation for the discrepancy of the result for argon found by Beall et al. is that the argon was contaminated with nitrogen, since the addition of as little as 1% of nitrogen to argon is known to increase the electron drift velocity fivefold.

Fischer and Zorn, as a result of their measurements, concluded that the electron drift velocities in argon-alcohol and helium-alcohol mixtures are the same. They attributed this to the overwhelming effect of the alcohol. It is therefore interesting to enquire if alcohol has such an effect on the drift velocities of

electrons in neon. Fig. 19 shows that this is not the case, and that electron drift velocities in a neon-alcohol mixture are greater than those in either an argon-alcohol or helium-alcohol mixture.

On comparing the present results with those for pure neon given by von Engel (1955), it is apparent that the presence of alcohol (and the impurities present in the neon used in the present experiments, see table 2) caused a general increase in the drift velocities of electrons in neon. The more recent work of Bowe (1960) indicates drift velocities in pure neon which are less than those of von Engel, and therefore the effect of the alcohol or impurities in the neon could be even more marked than indicated in fig. 19.

With regard to the internal consistency of the present data and the applicability of the suggested model, it is concluded that all the characteristics except that of the variation of mobility with rise time are in accord withexpectation. Part of the inconsistency for the rise time variation can be explained in the following way. Pulses having long rise times generally do not reach their maxima before the spark occurs and as a result the mean electron mobility becomes weighted towards the value for small fields and the drift velocity is correspondingly higher. All the apparent variation of $\overline{K[E(T_F)]}$ with rise time cannot be explained in this way, however, and in this respect the proposed model requires further improvement.

4.2 Geometrical Properties of the Sparks

4.2a The angle between the spark and the particle trajectory

Many workers have observed sparks tending to lie along the direction of the particle trajectory even when this is not normal to the plates. The usefulness of the chamber would be increased if it could be arranged that the direction of the spark were always to lie along the particle trajectory. Accordingly, measurements have been made to study the relationship between the conditions of operation and the inclination of the spark.

For each event in which one spark was produced by an ionising particle in at least five of the six sensitive gaps of the chamber the tangents of the angle θ between the particle trajectory and the applied field, and the angle θ_1 between each spark and the field were measured.

To indicate the fluctuations of $\tan\theta_1$ for a fixed $\tan\theta$ the frequencies of individual values of $\tan\theta_1$ are given in Fig. 20 for two pulse amplitudes for the range $0.45 \geqslant \tan\theta \geqslant 0.35$. Table 4 shows the magnitudes of these fluctuations.

Table 4. Fluctuations of the angle of an oblique spark due to a particle traversing the chamber at an angle θ, $0.45 \geqslant \tan\theta \geqslant 0.35$.

(a)	(b)	(c)	(d)
7	50	0.075 ± 0.005	0.13 ± 0.01
11.6	45	0.061 ± 0.005	0.16 ± 0.01

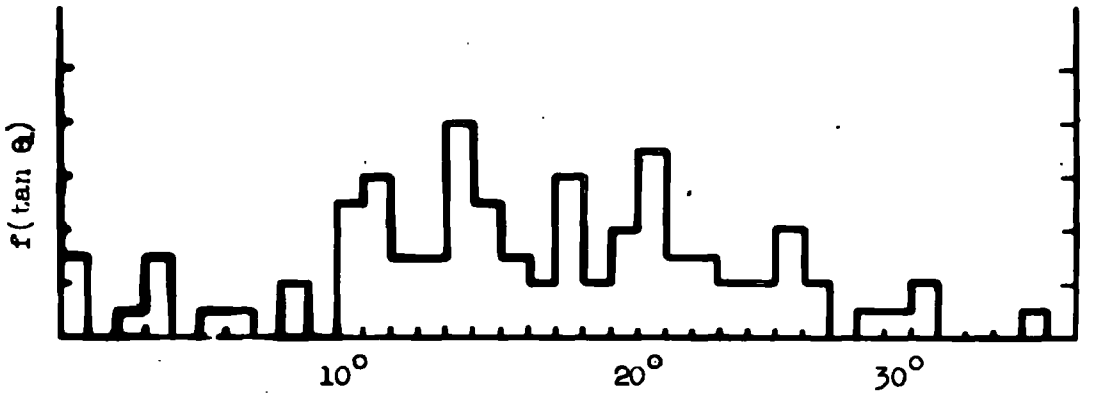

Pulse height = 7 kv cm^{-1}, T_R = 50 nsec

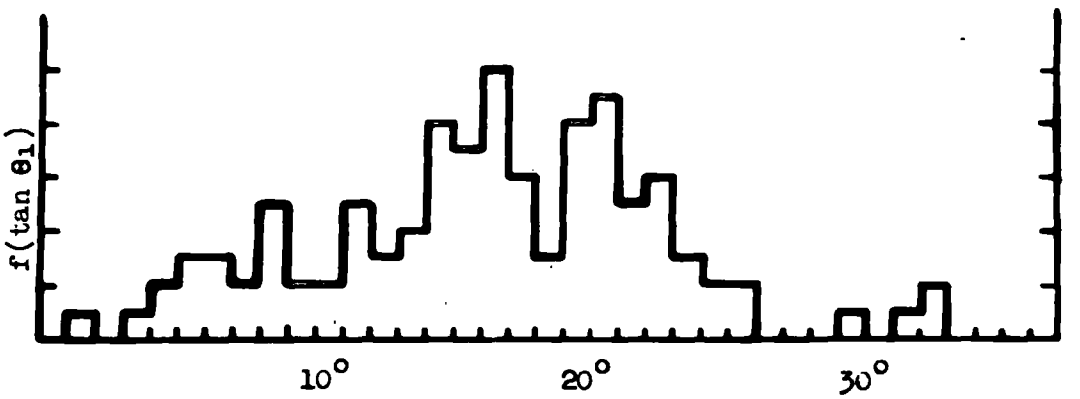

Pulse height = 11.6 kv cm^{-1}, T_R = 45 nsec

Fig. 20. Frequency distributions of tan θ_1 for a fixed tan θ for two pulses.

(a) pulse height (kV cm^{-1}); (b) rise time (nsec); (c) standard deviation of $\tan\theta_1$ from the mean; (d) mean $\tan\theta_1$.

The values in the table indicate that the variation of the angle of the spark for a fixed particle trajectory probably decreases with increasing voltage, but that even at overvoltages of the order of 200% there is still a very large fluctuation in the angle of the spark.

In view of this large fluctuation, the mean value of $\tan\theta_1$, $\overline{\tan\theta_1}$, for the five or six sparks on each particle trajectory, rather than each value of $\tan\theta_1$, is plotted against $\tan\theta$ in fig. 21, for a pulse of rise time 45 nsec and amplitude 11.6 kV. From this figure it is seen that there is a maximum angle of the spark of about 23° for a trajectory at $\sim 40^\circ$.

In order to compare similar curves for various pulse amplitudes and rise times, a straight line has been fitted to points below $\tan\theta \simeq 0.6$ with the result that in this range the ratio $(\overline{\tan\theta_1})/(\tan\theta) = 0.39$. Table 5 gives the ratio for various pulses and counter fillings of commercial neon alone and the usual neon-alcohol mixture.

On comparing the results for the neon and the neon-alcohol fillings, for similar pulse characteristics, it is evident that the addition of alcohol to neon does not affect the ratio $(\overline{\tan\theta_1})/(\tan\theta)$ appreciably. The measurements at 7 kV cm^{-1} indicate

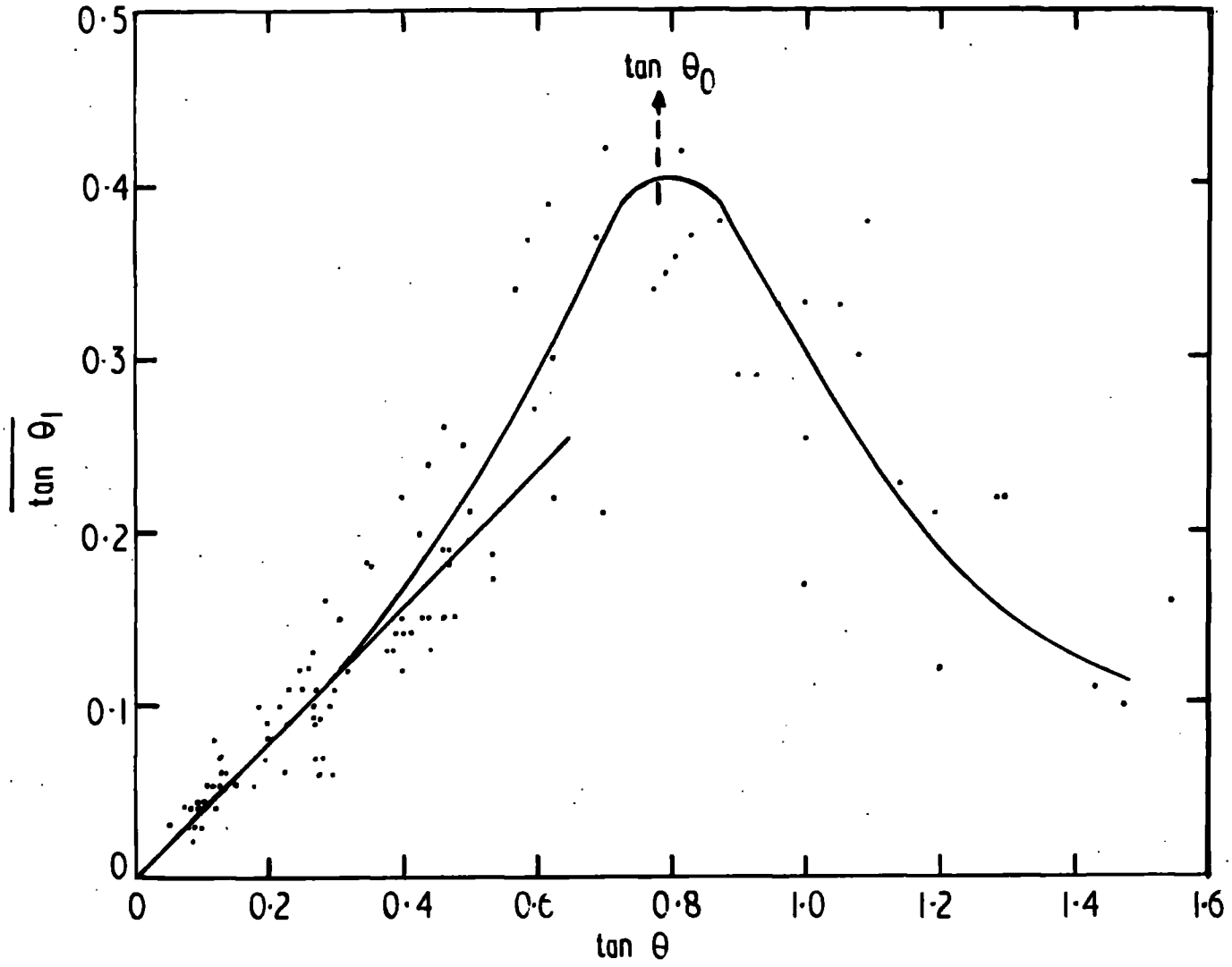

Fig. 21. The mean value of tan θ_1 (for each particle) as a function of tan θ (T_R = 4.5 nsec, pulse height = 11.6 kV).

Table 5. The maximum angle of the sparks for various pulse parameters

	(a)	(b)	(c)	(d)	(e)
Neon	7	40	0.27 ± 0.05	-	-
	9.2	50	0.37 ± 0.09	-	-
Neon-alcohol	7	80	0.13 ± 0.02	0.22 ± 0.02	0.70 ± 0.1
	7	50	0.34 ± 0.03	0.31 ± 0.02	0.80 ± 0.1
	9.2	50	0.40 ± 0.02	0.38 ± 0.03	0.75 ± 0.1
	11.6	45	0.39 ± 0.02	0.42 ± 0.02	0.80 ± 0.1

(a) pulse amplitude (kV cm^{-1}); (b) rise time (nsec); (c) $(\overline{\tan\theta_1})/\tan\theta$); (d) maximum value of $\tan\theta_1$; (e) value of $\tan\theta$ at maximum value of $\tan\theta_1$, i.e. $\tan\theta_o$.

that pulses having a long rise time do not favour the production of sparks at large angles. Increasing the amplitude of the pulse does not greatly affect the ratio $(\overline{\tan\theta_1})/(\tan\theta)$, but the maximum angle at which a spark can be produced in slightly increased.

4.2b The width of the spark

The width of the spark has been investigated as a function of the angle between the trajectory of the particle and the direction of the applied electric field for various pulse amplitudes and rise times.

The results shown in Fig. 22 indicate that for a pulse of rise time 60 nsec particles which pass through the chamber vertically produce sparks whose widths are about 1.5 mm independent of pulse amplitudes. For particles traversing the chamber at larger angles,

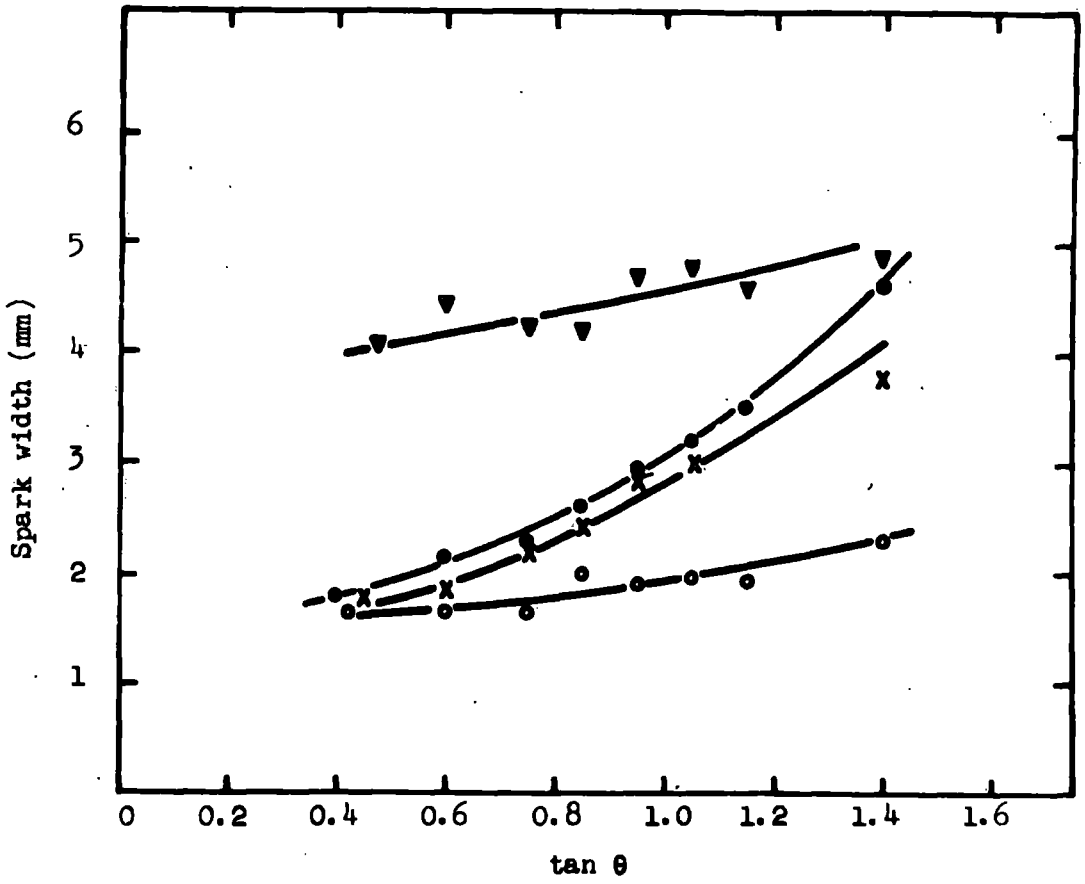

Fig. 22. The width of the spark as a function of the angle of the trajectory for various amplitudes and rise times.

however, the widths of the sparks increase with increasing applied voltage.

For angles below 55° the sparks do not usually exhibit a multiple structure, but at greater angles two or three sparks in the direction of the applied field are produced in each gap on the particle trajectory.

4.2c The accuracy with which the spark locates the particle trajectory

The accuracy of track location was studied by examining only those photographs corresponding to particles of energy >500 MeV, because for such particles the scattering in the aluminium plates of the chamber could be neglected. Furthermore, only those photographs which included at least one spark in each of the six gaps, and which corresponded to particles travelling within 20° of the field direction, were accepted. For the events satisfying these criteria the deviation, δ, of the centre of each individual spark at its (pulsed) cathode end from the best straight line passing through the six such points was recorded. Fig. 23 shows the histogram so obtained. The distribution has an r.m.s. value of 0.37 mm, a median of 0.22 mm and a mean value of 0.27 mm.

So that an estimate of the uncertainty in the measurement of δ could be made the measurements were repeated, and the frequency distribution of the difference between successive measurements was

drawn. This was found to have an r.m.s. value of 0.34 mm and it is estimated that the broadening of the distribution of fig. 23 due to this latter uncertainty is of the order of that produced by a Gaussian distribution of standard deviation $0.34/\sqrt{2}$. Hence, the distribution of the displacement of the cathode end of the spark from the particle trajectory has an r.m.s. value of approximately 0.28 mm.

The measurements have also been repeated by setting on the mid-point and anode end of the sparks with the results given in Table 6.

Table 6. Accuracy of location of sparks relative to the apparent trajectory of the ionising particle

	(a)	(b)	(c)
R.M.S. value	0.37 ± 0.02	0.26 ± 0.03	0.30 ± 0.03
Mean value	0.26 ± 0.03	0.17 ± 0.02	0.19 ± 0.03
Median value	0.22 ± 0.03	0.15 ± 0.02	0.14 ± 0.02

(a) cathode end of spark (mm); (b) mid-point of spark (mm); (c) anode end of spark (mm).

The magnitudes of the displacements given in the table are consistent with the distance an electron diffuses during the time delay in applying the high voltage pulse. (In 0.5 μsec an electron

diffuses a mean distance of the order of 0.5 mm. The position of the spark is, however, probably dependent upon the position of several electrons and its displacement is therefore expected to be less than this). These results do not refer to the accuracy with which the sparks define the true position of the trajectory of a particle since there may be a systematic displacement of the mean spark position from the trajectory. There is no evidence for this, and even if there were, in many experiments the systematic component is unimportant.

The present results, numerically consistent with those of other workers (see §1.3f, page 11), indicate that the fluctuation of the mid-point of the spark about its mean position is less than that of either end. Because of the interaction between evalanches in the centre of the gap the position of the mid-point of the spark depends upon the point of production of several electrons. At the cathode and anode ends the position of the spark depends solely on the point of production of a single electron. As a result there will be some region of the spark whose displacement from the actual particle trajectory is relatively more constant than that of the ends of the spark. This is consistent both with the present work and that of Mikhailov et al.

The conclusion is, therefore, that when the direction of a particle trajectory is to be measured, better accuracy is obtained

by recording the centre of the spark than either end, but if the actual particle trajectory is required the most accurate direct estimate is obtained from the cathode end of the spark.

4.2d Conclusions about the model of the discharge

In this section it will be shown that, in the main, the experimental results support the mechanism of the discharge outlined in §2.1 and §2.2. There it was proposed that when the radial space charge field, E_r, produced by the positive ions at the head of each avalanche attains a value of the order of the applied field, E, mid gap streamers can be formed and the discharge will then grow by the streamer mechanism.

E_r can be estimated on the assumption that the positive ions at the head of an avalanche are contained in a spherical volume of radius r. Raether (see Meek and Craggs, 1953) gives the value of E_r, the radial field due to a single avalanche, as

$$E_r = \frac{e}{r^2} \exp(\alpha x)$$

where e is the electron charge and r is the radius of the avalanche after it has travelled a distance x; following Raether, r is given by the expression $r = \sqrt{3Dt}$, D is the diffusion coefficient and t is the time of development. Thus

$$E_r = \frac{e}{3Dt} \exp(\alpha x) \qquad (4)$$

The transition from an electron avalanche to a streamer occurs when $E_r = cE$; c being taken to lie in the range 0.1 to 1.0 using equation (4) the striking potential for a particular gas can be estimated provided that both t and α are known as a function of the field $\bar{E}$. Taking x equal to the gap width, t from figure 10, D from Lloyd (1960) and the value of α as measured by Kruithof and Penning (1937) for neon containing 10^{-4} % argon, E_r has been calculated for a pulse of rise time 40 nsec. Values of E_r are given in table 7.

Table 7. Radial field of an avalanche after travelling 1 cm in the applied field

Applied field, E	Radial field, E_r
v cm^{-1}	v cm^{-1}
3,000	3.5
3,500	5.4
4,000	1,200
5,000	25,000

It is apparent that streamers are expected to be produced in the gas at a minimum applied field, E, in the region of 4 kV cm^{-1}. This is consistent with the directly measured value of 3.5 $\pm$ 0.5 kV cm^{-1}, and the agreement supports the suggested mechanism.

4.2e Interpretation of the geometrical properties of the sparks

The sparks due to particles traversing the chamber at an angle are, in the main, either straight or concave with respect to the cathode. For particles traversing the chamber at an angle less than $\theta_o \simeq 40^o$ (figure 21) the great majority of the sparks are concave, whereas for angles greater than θ_o the majority of the sparks are straight. The shape of the spark predicted by the reasoning of §2.2 is shown in Fig. 5c. From photographs obtained with the chamber, some of which are shown in figures 25 to 32, it may be seen that the general shape of the sparks is in agreement with the predicted one.

It can be shown that for a particle traversing the chamber at an angle $\theta(\theta<\theta_o)$ to the vertical, the angle θ_2 of fig. 24 is given by

$$\frac{\tan\theta_2}{\tan\theta} = (1 - \frac{x}{d}) \qquad (5)$$

In the figure, the particle produces electrons along AB; these electrons produce avalanches which become critical after travelling the distance x. Assuming that the spark lies in the direction BC, it is natural to attempt to identify θ_2 with θ_1 of §4.2a. For a pulse of amplitude 7 kV and rise time 60 nsec, x from equation (5) is ~6.6 mm, and this is in good agreement with the value of 6 mm calculated from the measured spark formation time, T_F, and the mean electron mobility $\overline{K[E(T_F)]}$.

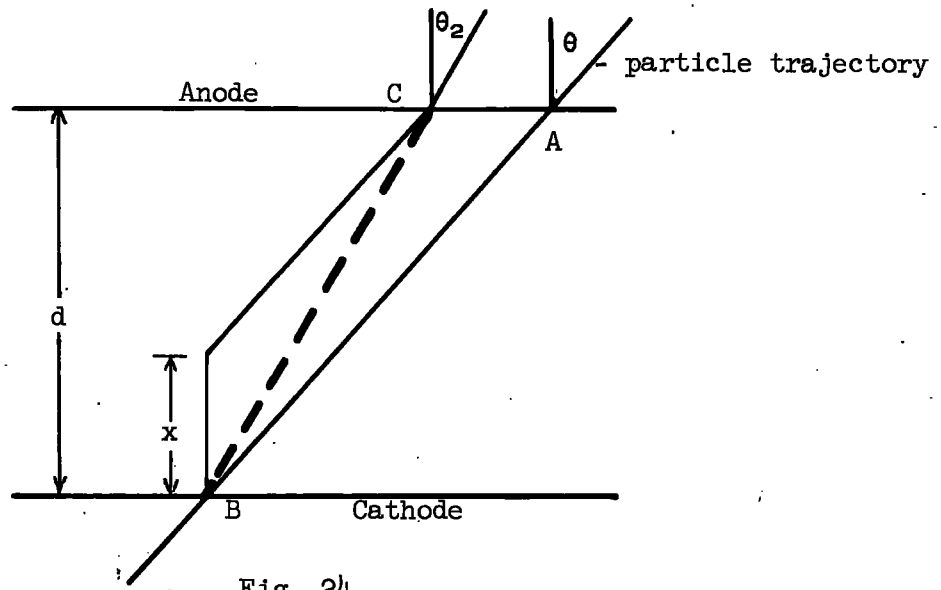

Fig. 24

Geometrical property of the spark.

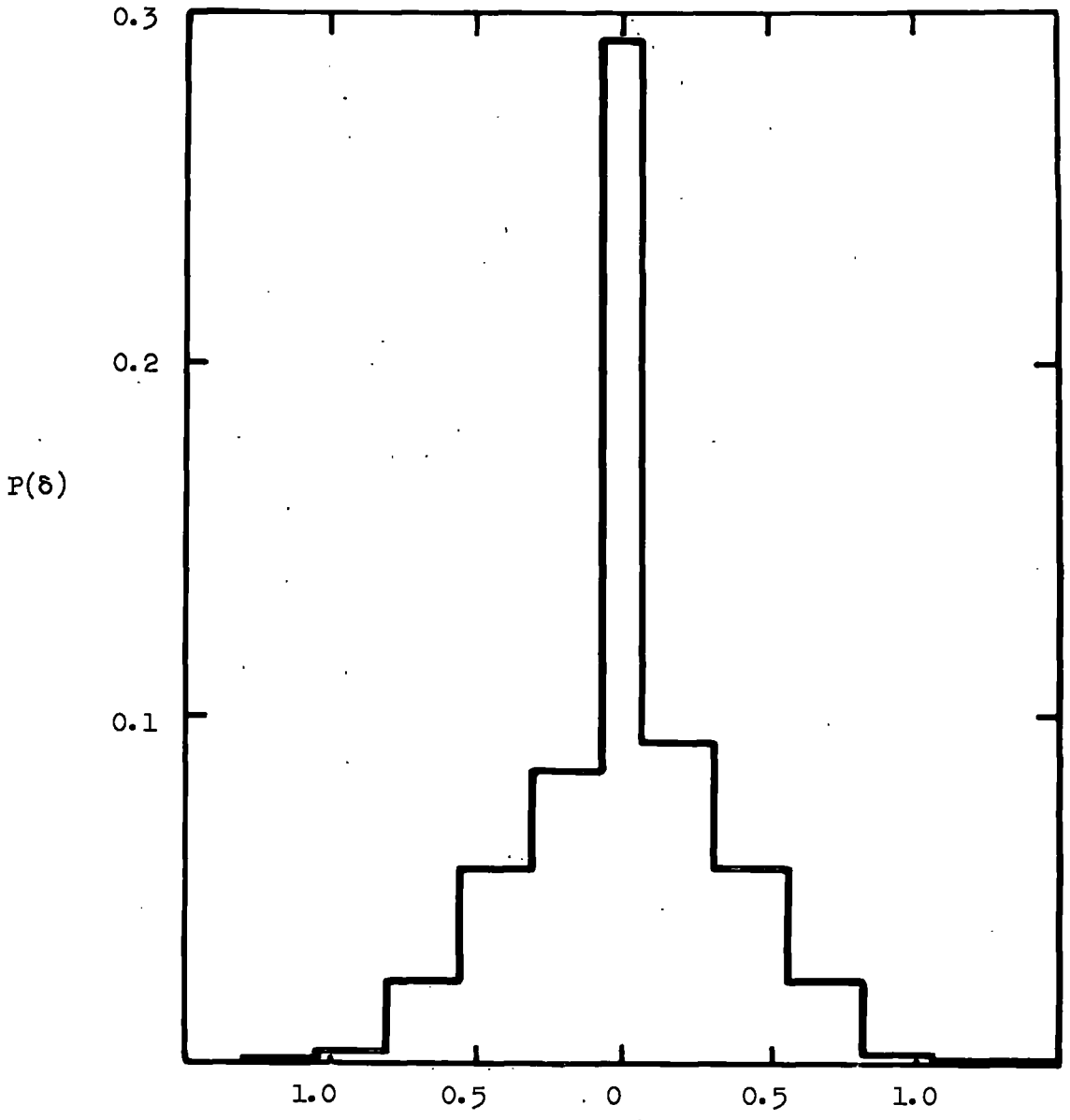

Fig. 23 Frequency distribution of δ, the displacement of the spark discharge from the estimated particle trajectory

The presence of a maximum in the $\overline{\tan\theta_1}$ vs. $\tan\theta$ curve (figure 21) can be explained on the basis of interaction between the elementary avalanches. For small values of θ the avalanches interact strongly and the spark passes effectively through the avalanche heads (fig. 5c). At larger values of θ the separation of the avalanches is so great that interaction ceases and the direction of the spark tends to be set by the motion of the electron initially nearest the cathode, i.e. θ_1 is reduced.

The electrons produced in the neon-alcohol mixture by an ionising particle are on the average 0.5 mm apart, and so the maximum angle of a spark will be in the region of $\sin^{-1}\frac{\sqrt{2Dt}}{0.5}$ (where D is measured in $mm^2 sec^{-1}$). This neglects any retarding effect which the growth of one avalanche may have on its neighbour and so the maximum angle could be less than that given above. For the case of an 11.6 kV pulse of rise time 45 nsec $t = T_F \simeq 50$ nsec (fig. 10), so that the maximum angle of the spark is approximately $\sin^{-1} 0.35 = 21^\circ$. This is in remarkably good agreement with the observed value of $\tan^{-1} 0.42 = 23^\circ$ given in table 6.

4.2f Photographs obtained with the chamber

The results presented so far have been obtained with the six-gap chamber described in §3.1. A nine-gap chamber was also constructed. This was used to obtain the results presented in section 4.3 In the nine-gap chamber the planes of all plates were parallel and alternate plates were connected in parallel so that here no insensitive gap was produced. The sensitive area and width of the gap were the same,

i.e. 4.3 x 16.5 cm^2 and 1 cm respectively, and ebonite was used instead of perspex to support the plates. Figs. 25, 26, 27, 28 and 29 show typical photographs obtained with the first chamber, and figs. 30, 31 and 32 were obtained with the nine-gap chamber. The laterally inverted "L" seen in the photographs is a frame indicator.

The concave nature of the sparks can be clearly seen on the angled tracks.

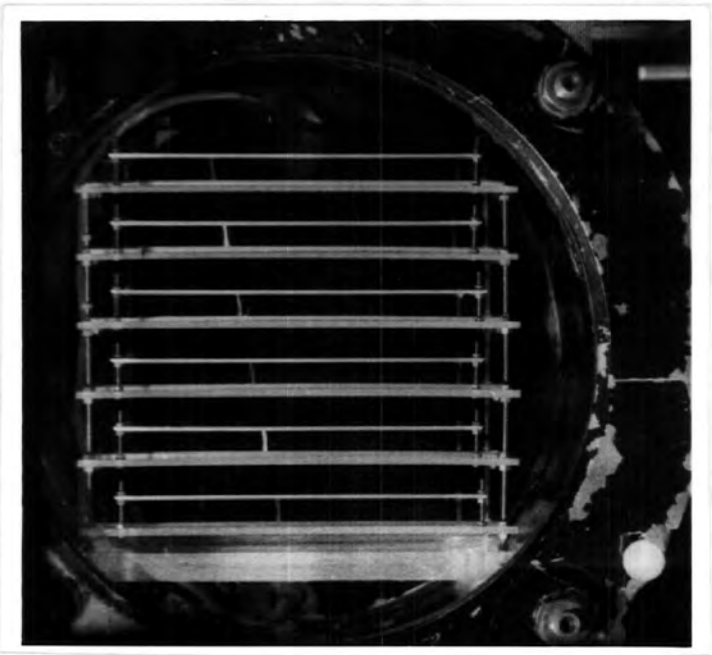

Fig. 25. A single particle traversing the chamber.

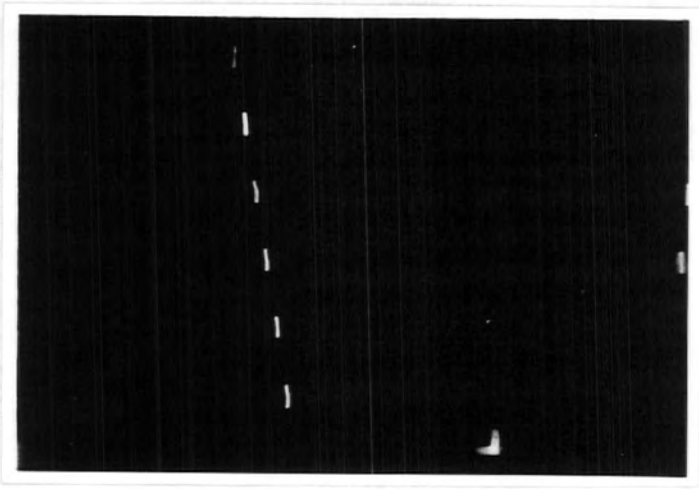

Fig. 26. A Single Particle

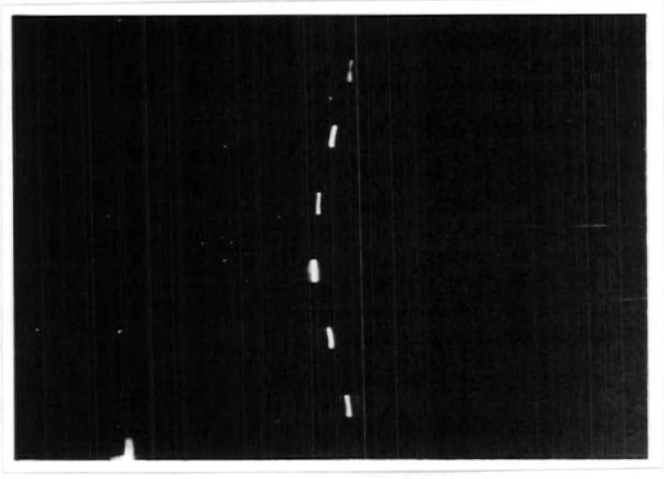

Fig. 27. A particle scattered in the aluminium plates of the chamber

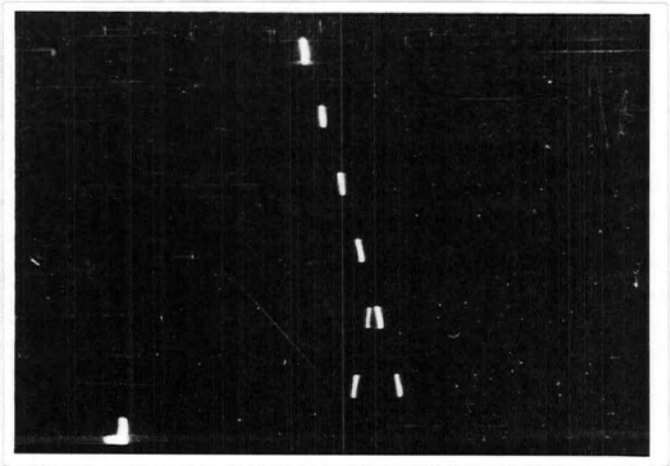

Fig. 28. A knock-on electron produced by the cosmic ray particle is seen in the lowest 2 gaps

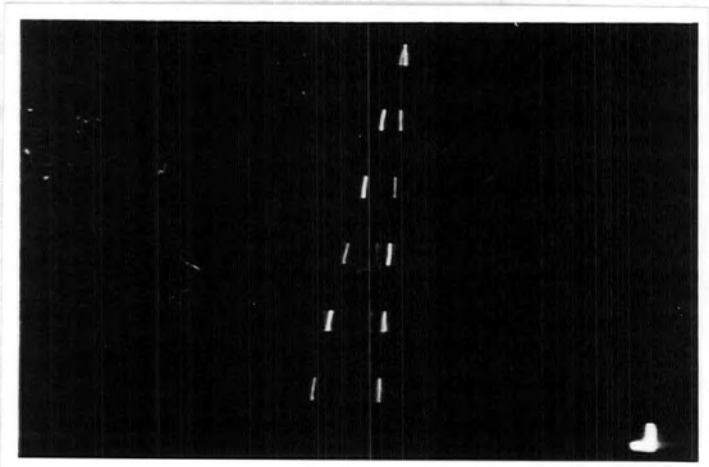

Fig. 29. A knock-on electron produced in the first electrode. Note the definition in the first gap

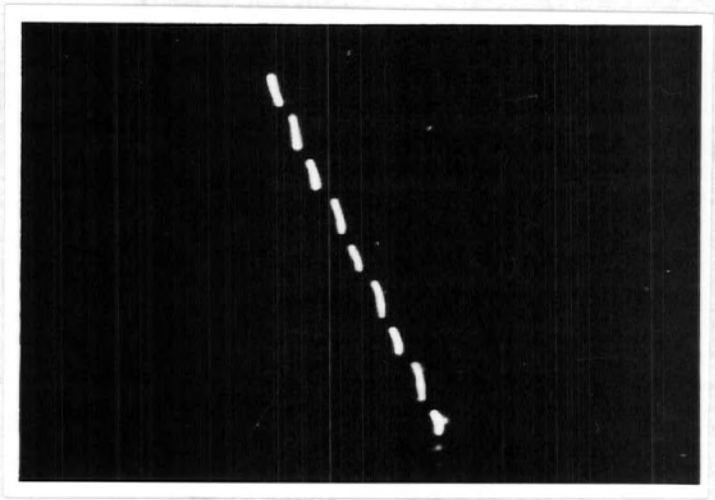

Fig. 30. Track of a single particle

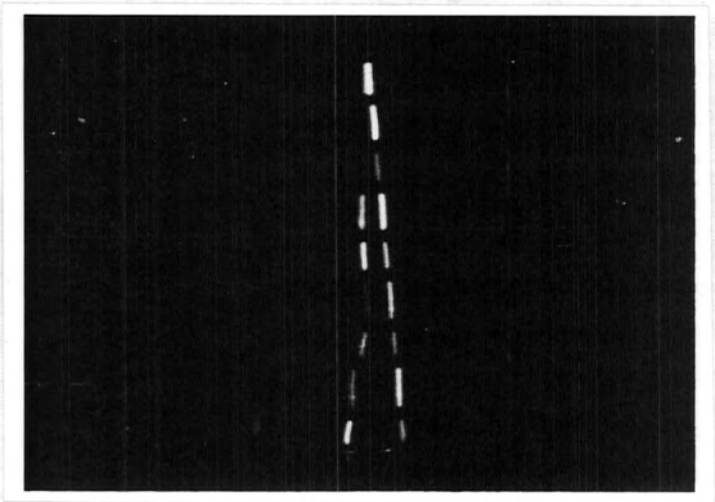

Fig. 31. A knock-on electron produced in the third gap

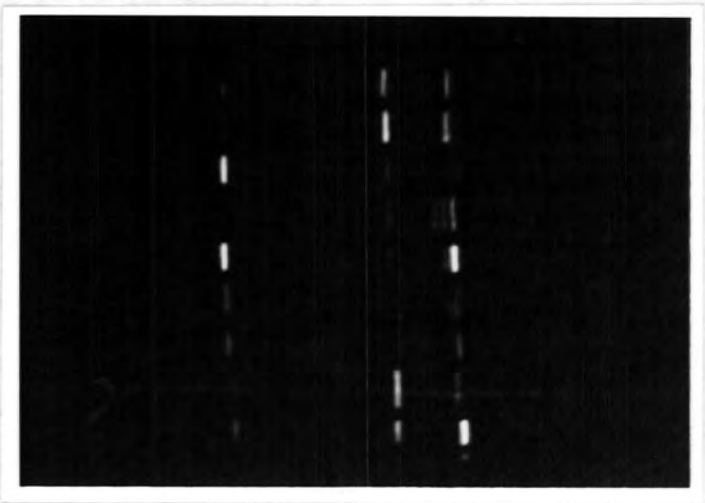

Fig. 32. A cosmic ray shower event in which three particles traversed the chamber simultaneously

4.3 The Effect of Electron Attachment by Impurities in the Chamber

In this section the effect of the addition of air on the efficiency of the chamber is considered.

Small amounts of air were admitted to the nine-gap chamber which was filled with commercial neon only, i.e. no alcohol was present in the gas. The efficiency of the chamber for recording single particles was measured as a function of the time delay for zero clearing field. The results are shown in Fig. 33.

The theoretical efficiency is given by

$$\eta = 1 - \exp(-fn_2)$$

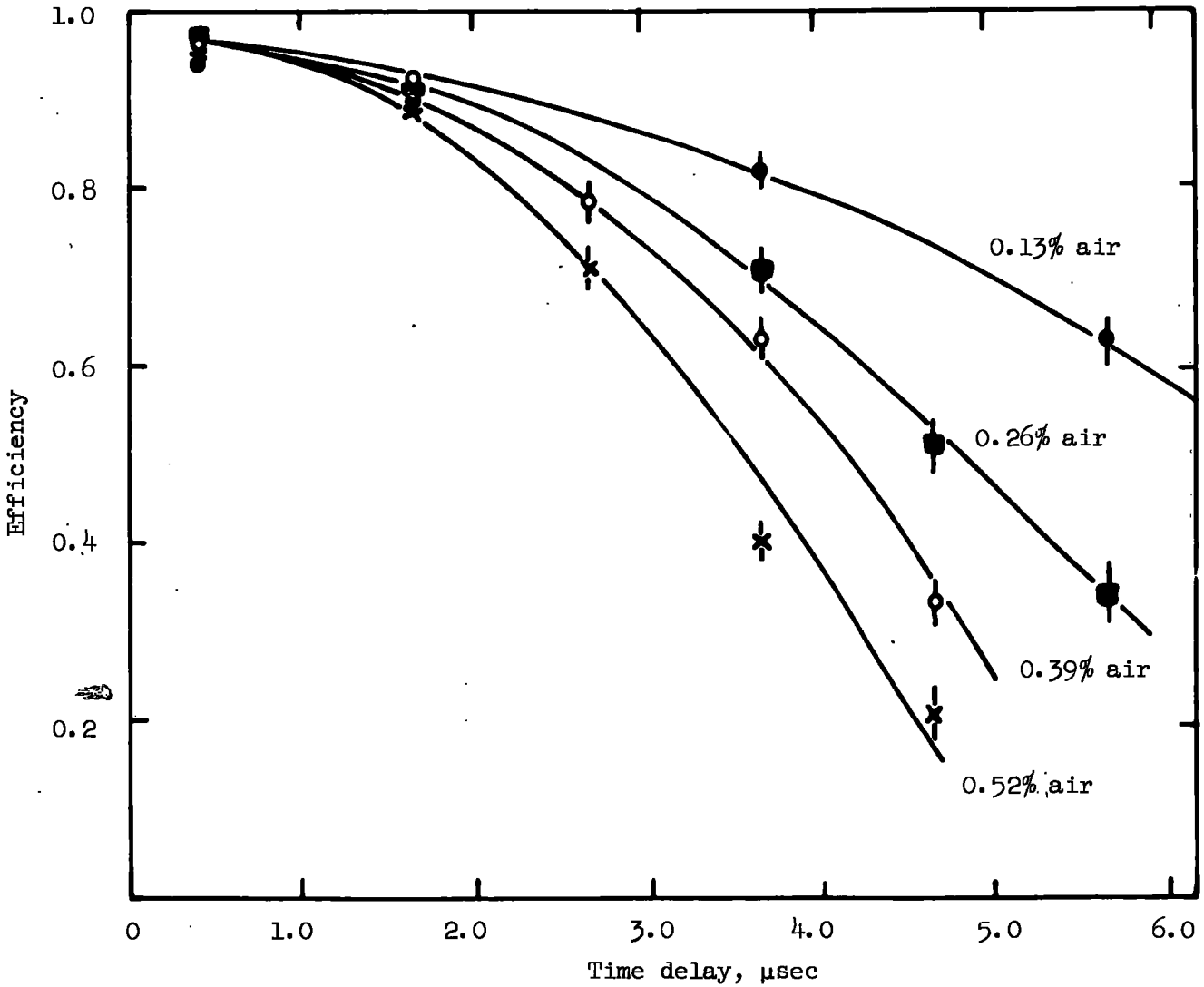

Figure 33. The efficiency as a function of the time delay for various impurity concentrations

where n_2 is the number of primary electrons capable of initiating avalanches, which can grow to the critical size, remaining between the plates at the instant the high voltage pulse is applied (see §2.3). The factor f, the probability that a single electron will escape attachment during the pulse, is taken to be 0.25 from §4.1b.

In order to estimate the effect of electron attachment during the time delay in applying the high voltage pulse, all processes by which electrons are removed from the gap must be considered separately.

(a) Diffusion

It is assumed that the electrons produced by the triggering cosmic ray particles are equally spaced in the x direction perpendicular to the plates. For an average number, $n_o = 20$, the distance between adjacent electrons will be 0.05 cm. Those electrons which reach an electrode by diffusion are considered to be removed from the gap. The probability of an electron produced at x = 0 at time t = 0 having at a later time t = t an x component of displacement between x and x + dx is given by

$$P(x)dx = \frac{1}{\sqrt{4\pi Dt}} \exp\left(-\frac{x^2}{4Dt}\right) dx$$

D is the diffusion coefficient for electrons in neon at one atmosphere and is given by Lloyd (1960) as $D = 1800\ cm^2 sec^{-1}$. If the positions of the electrodes relative to an electron at x = 0 are described by $x = x_o$ and $x = x_o - 1$ then the probability of this electron being lost to either of the electrodes is given by

$$P_{loss} = 1 - \int_{x_0-1}^{x_0} \frac{1}{\sqrt{4\pi Dt}} \exp\left(-\frac{x^2}{4Dt}\right) dx.$$

P_{loss} was evaluated individually for each of the 20 electrons for various values of t. The result was that the number of electrons, n_D, removed from the gap in a time t is well represented by the relationship

$$n_D = 0.95 \sqrt{10^6 t} \quad \text{for} \quad 10^{-6} < t < 6 \times 10^{-6} \text{ secs}$$

(b) The clearing done by the pulse

A further fraction, g, of the electrons present at the instant of application of the high voltage pulse will be captured by the electrodes due to the clearing action of the pulse. For the pulse used in this experiment (pulse height, 7 kV; rise time, 12 nsec; decay time, 180 nsec) this fraction, given by

$$g = \int_0^{T_F} \frac{\omega[E(t)]dt}{d}$$

was $g = 0.3 \pm 0.1$.

(c) Attachment during the time delay

The probability of an electron being attached during the time delay, T_D, depends on the number of collisions it makes with impurity atoms or molecules. The time delay comprises two parts:- a period in which the initial electrons of average energy of about 6 eV slow down to thermal energies, and the remaining period in which they move with thermal velocities. Heyn (1961) has shown the former

period to be ~0.5 μsec, and it is assumed that the number of collisions an electron makes in this time is constant and is given by $N_1 \simeq 8.3 \times 10^4$. According to kinetic theory a thermal electron in neon at atmospheric pressure makes 1.32×10^{11} collisions per second. Thus, with an impurity concentration of y% the total number of collisions an electron will make with impurity molecules in the time T_D is

$$N_{total} = \frac{N_1 y}{100} + 1.32 \times 10^9 \ (T_D - 0.5 \times 10^{-6})y$$

If a is the probability of attachment per collision for thermal electrons and ka is the probability of attachment per collision for electrons during the slowing down period, the number of electrons, n_A, remaining after a time T_D is given by

$$n_A = n_o \exp\left\{-ay\left[\frac{kN_1}{100} + 1.32 \times 10^9 \ (T_D - 0.5 \times 10^{-6})\right]\right\}$$

Consequently the number of electrons, n_2, remaining in the gap after a time T_D is

$$n_2 = (n_A - n_D)(1 - 0.3)$$

$$i.e. \quad \eta = 1 - \exp\left\{-\tfrac{1}{4}(n_A - n_D)(1 - 0.3)\right\}$$

$$i.e. \quad \ln\frac{1}{1-\eta} = \frac{0.7 \times 20}{4}\exp\left\{-ay\left[\frac{kN_1}{100} + 1.32 \times 10^9 (T_D - 0.5 \times 10^{-6})\right]\right\} - \frac{0.7 \times 0.95}{4}\sqrt{10^6 T_D}$$

$$or \quad \ln\left\{\ln\frac{1}{1-\eta} + 0.166\sqrt{10^6 T_D}\right\} = 1.25 - \left[\frac{kN_1}{100} + 1.32 \times 10^9 (T_D - 0.5 \times 10^{-6})\right]ay \qquad \ldots\ldots (6)$$

Fig. 34 shows the left-hand side of equation (6) plotted against y with T_D as parameter. The gradients, s, of the straight lines were calculated by the method of least squares to form six equations of the form

$$s_i = 1.32 \times 10^9 (T_{D_i} - 0.5 \times 10^{-6})a + \frac{kN_i a}{100}$$

Fig. 35 shows s plotted against $1.32 \times 10^9 (T_D - 0.5 \times 10^{-6})$. The six points lie on a straight line whose slope and intercept were calculated by the method of least squares to yield $a = 6.6 \times 10^{-5}$ and $k = 0.75$. This means that the probability of attachment for thermal electrons is four thirds that of those slowing down from an average energy of about 6 eV.

The value of a obtained in this experiment is an order of magnitude greater than the value of $a = 0.5 \times 10^{-5}$ for air given by Compton and Langmuir (1930), and an order of magnitude less than that observed by Wilson (1950) for electron attachment to oxygen impurity in an ionisation chamber. The results of Schneider and Höhne (1963), who measured the efficiency of an oxygen-contaminated spark chamber as a function of the electron energy for various delay times, point indirectly to a value of $a \lesssim 3 \times 10^{-4}$ for electron energies below about 0.2 eV, corresponding to $a \lesssim 6 \times 10^{-5}$ for air, since $a(\text{air}) = \frac{1}{5} a(O_2)$. This limit is barely consistent with the value reported here.

The fact that the points in figs. 34 and 35 lie on straight lines supports the validity of the present analysis and gives

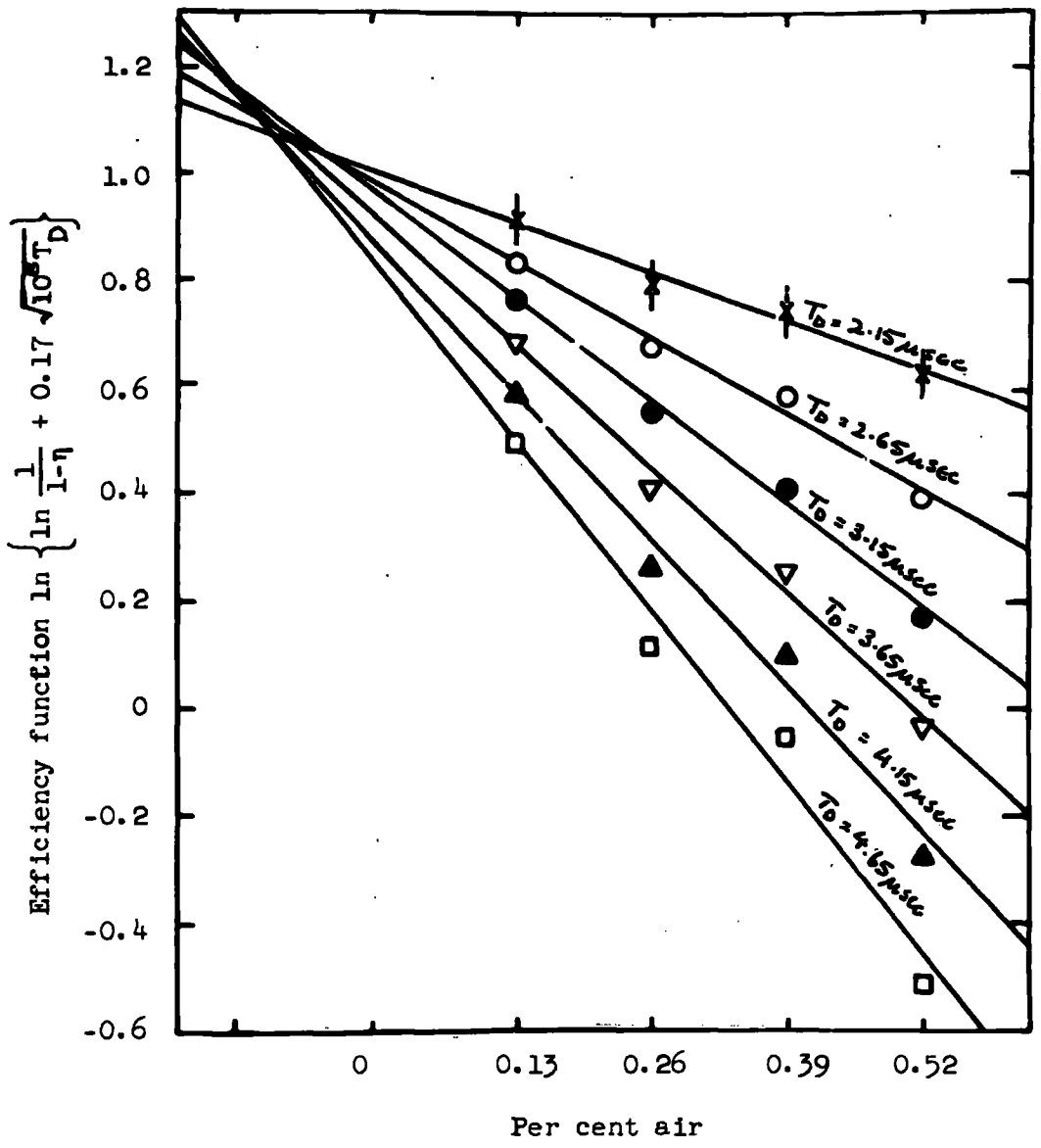

Fig. 34. The efficiency function $\ell n\left\{\ell n\frac{1}{1-\eta}+0.17\sqrt{10^6 T_D}\right\}$ as a function of the amount of impurity for various values of the time delay.

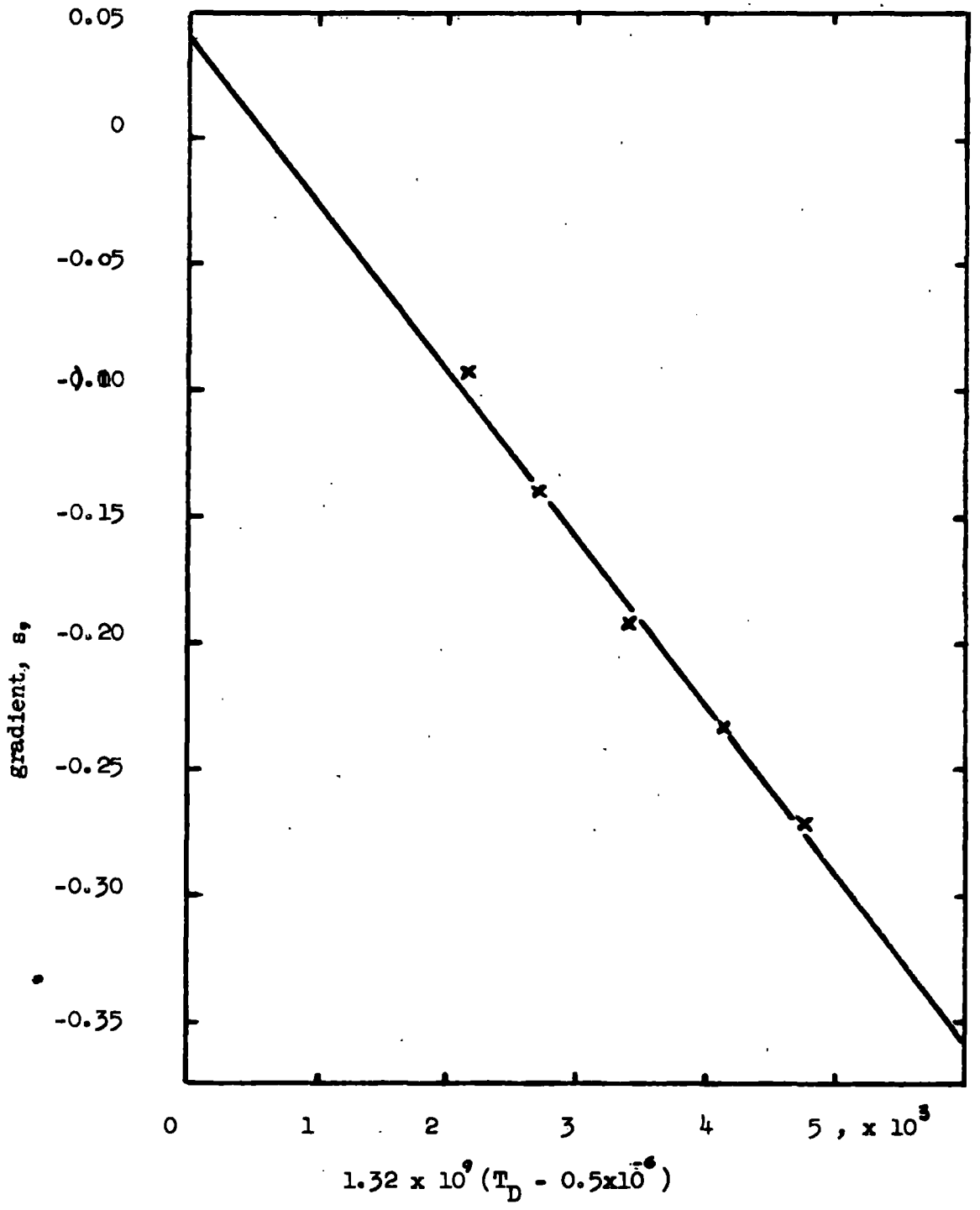

Fig. 35. The gradients, s, of the straight lines of fig. 2 plotted against the corresponding values of $1.32 \times 10^{9}(T_D - 0.5\times10^{-6})$.

added weight to the validity of the discharge model postulated in Chapter II. The region of the intersections in fig. 34 indicates that the equivalent of 0.1% air impurity was present in the chamber before additional air was introduced; this amount is considered reasonable.

4.4 Conclusions from the experimental results

The results have been used to determine the value of the electron drift velocity in a neon-alcohol mixture as a function of the electric field over the range of E/p from 0.05 to 4 v cm^{-1} $(mm\ Hg)^{-1}$.

The probability of a single electron initiating a spark has been measured under a variety of conditions and found to be internally consistent within the experimental error.

The accuracy with which the spark locates the particle trajectory has been measured and found to be in agreement with that observed by other workers. It is concluded that when the direction of a particle trajectory is to be measured, better accuracy is obtained by recording the centres of the sparks than their ends; but if the actual particle trajectory is required the most accurate direct estimate is obtained from the cathode end of the spark.

A model for the formation of the spark has been proposed. The interpretation of the variation of efficiency with the characteristics of the high voltage pulse augurs well for the validity of this model.

Measurements have been made to study the relationship between the condition of operation of the chamber and the tendency of the spark to lie along the particle trajectory if this is inclined at an angle to the normal to the plates. The presence of a maximum angle of inclination of the spark, and its magnitude, which agrees very well with that

predicted by the model, lend further support to its validity.

The effect of electron attachment on the efficiency of the chamber has been measured, the results supporting the present model, although being barely consistent with those of other workers. The problem of electron attachment in spark chambers has not yet been examined on a sound theoretical basis, and there is much scope for further work in this field.

The statistics of the electron avalanche leading to spark formation have not yet been worked out. It would be of interest to study this for a comparison to be made between the theoretical value of the spark formation time and the experimental one, as measured in these experiments.

Although a partial explanation has been advanced for the variation of electron mobility with rise time of the pulse further explanation is needed and the model needs improvement with respect to this.

A somewhat surprising conclusion that may be drawn from the observations is that the spark chamber is ideally suited to certain measurements of the behaviour of electrons in gases, as the present measurements of electron drift velocity and electron attachment have shown. A fuller exploitation of the spark chamber technique is to be expected.

In the next chapter conclusions on the design of spark chambers, from information gathered by other workers as well as the author will be presented.

Finally, in Chapter VI, the different types of spark chamber developed up to the present time will be reviewed.

CHAPTER V

Conclusions on the design of spark chambers

In this chapter conclusions on the design of a conventional parallel plate spark chamber will be presented. Spark chambers facilitate a wide freedom in general design which is sufficiently flexible to enable one to suit the design and construction of the chamber to the particular application for which it is required.

5.1 Construction

In the construction of multiplate assemblies the following five requirements must be satisfied:-

(1) The plates must be electrically insulated from one another,

(2) The gap spacing between neighbouring plates must be made as uniform as possible over the whole sensitive area,

(3) Precautions must be taken to prevent breakdown of the gap due to field emission in the regions of intense field at the edges and corners of the plates.

(4) The chamber must be gas-tight and capable of being filled with the desired operating gas,

(5) There must be an unobstructed view into at least two sides of the chamber to facilitate stereo-photography of the tracks.

Two kinds of construction are possible:-

(a) that in which the whole multiplate assembly is placed in a single gas-tight enclosure with transparent windows,

(b) that in which the plates are separated by transparent gas-tight insulating frames which enclose the desired operating gas.

In type (a) it is necessary to round off the edges of the plates to avoid spurious breakdown of the gap. It is thought by most workers that a radius of curvature of at least $\frac{1}{8}$" is required; this means that if solid plates are to be used, they must be $\frac{1}{4}$" thick. For many experiments this presents an undesirable amount of absorbing material between successive spark gaps. In this case two alternatives exist:- either the plates may be crossed (as in the chamber described in chapter III) so that the probability of spurious breakdown is reduced, or the plates may be made hollow (as described by O'Neill, 1961) with a consequent complication of construction.

In type (b) there is no need to round off the edges of the plates, since the noble filling gas invariably has a lower breakdown potential than air.

When a minimum cross-section of material is required, electrodes of thin aluminium foil may be used. These may be cemented to perspex frames acting both as spacers defining the gap width and as walls providing the gas-tight enclosure of the gap. Here the main problems are those of making a gas-tight seal between the electrodes and the frames, and of providing a suitable means of entry for the filling gas. When very thin plate or foil electrodes are to be used, the additional problem of keeping them perfectly flat must be solved.

Aluminium is the most widely used material for the electrodes, but Fischer and Zorn (1961) found that any relatively smooth conducting material may be used for the plates. For instance, graphite plates sprayed with silver paint to prevent the formation of carbon dust by the sparks have been used by Cork (1961) and Cronin (1961).

Various methods of sealing have been described, some using epoxy resin or some other suitable cement (Meyer and Terwillinger, 1961; Fischer and Zorn, 1961; Lederman, 1961; Rutherglen and Paterson, 1961) and some using O-ring gaskets (Lederman, 1961). The former method has the advantage of simplicity of construction, but difficulties can arise due to the strains produced by the differential expansion of frames and electrodes. The latter method has the advantage that individual units may be added as desired and target material placed between them if required.

A simple O-ring method of construction has been described by Rutherglen (1963). It consists of stretching four well-greased rubber bands over the edges of perspex frames, assembling the plates and frames alternately, and clamping the assembly together. No difficulty was experienced in applying sufficient clamping force to make a seal at the corners, where one band crosses over another. Complete chambers constructed by Rutherglen in this way are shown in Fig. 36.

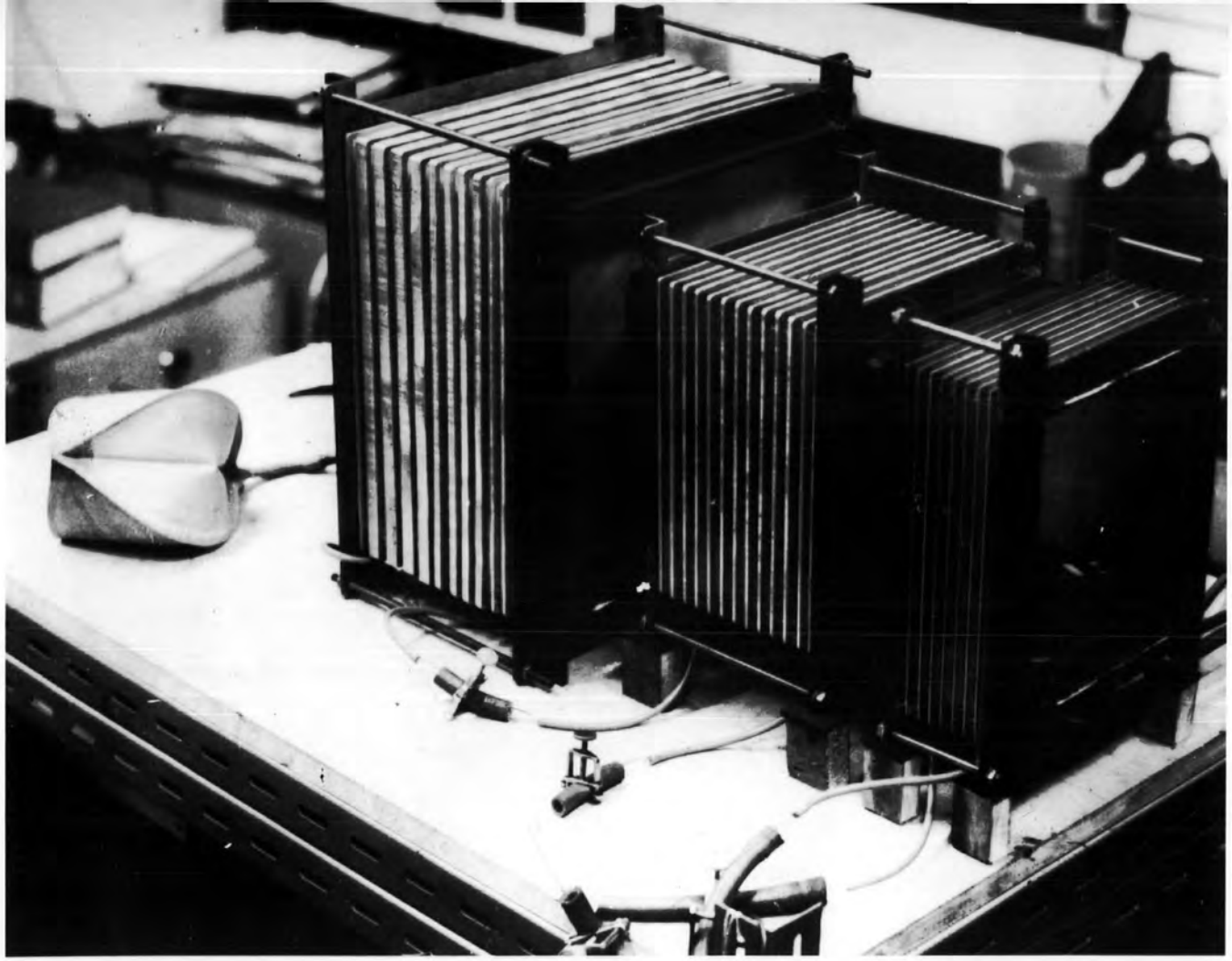

Figure 36. Chambers constructed by Rutherglen using a simple O-ring method.

Rutherglen also found that small holes maybe drilled through the plates without producing any tendency to cause spurious sparking. This enables the whole chamber to be filled with gas by allowing it to flow through inlet and outlet tubes sealed into the edges of the first and last perspex frames.

Chambers with aluminium foil electrodes as thin as 0.001" have been described by Fischer and Zorn (1961) and Meyer and Terwillinger (1961). It was necessary to keep the foil electrodes under tension to ensure that they would be flat. Both groups found that a satisfactory method of achieving this was to cement the foil to the perspex frames at a reduced temperature of 55° - 60°F; the thermal coefficient of expansion of perspex is about three times that of aluminium, so that the differential expansion pulled the foils flat to within 0.004" on returning to room temperature. One important limitation of thin foil spark chambers is that the foil may easily become damaged by the excessive energy discharged in the spark.

The methods of making the electrical connections are considered in section 5.3.

5.2 Electronics

The electronic circuits which are employed in the operation of a spark chamber may be divided into two parts, (a) the event selection system and (b) the high voltage pulse generator.

The event selection system normally consists of scintillation or Cerenkov counters coupled to the appropriate pulse height dis-

criminator and coincidence circuits, which serve to define the event for which the spark chamber is required to give a visual record or spatial information.

The details of these circuits will not be considered here, but it is important to emphasise that they should be so designed that the delay between the passage of the ionising particle through the chamber and the appearance of the pulse which triggers the high voltage pulse generator is a minimum.

The high voltage pulse is normally obtained from a triggered high voltage pulse generator thus ensuring a standard pulse shape independent of the variations of the input pulse from the event selection circuits.

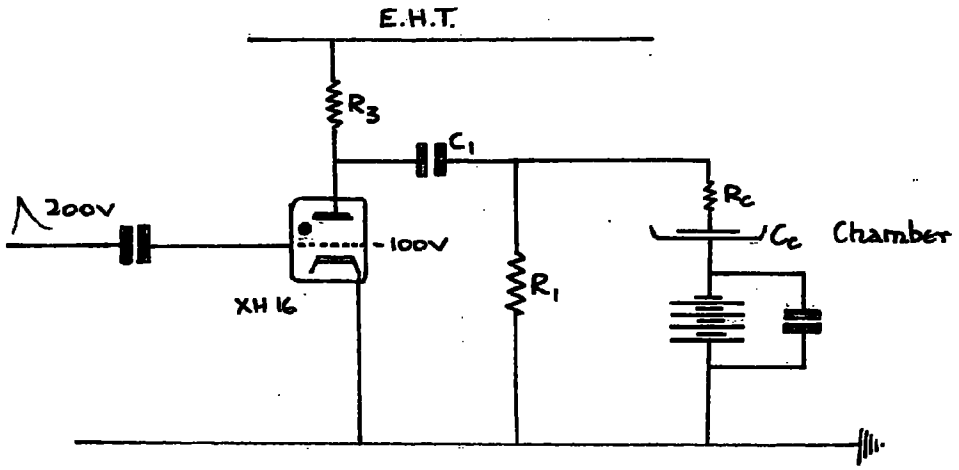

Fig. 37. Typical pulse generator circuit

The pulse generator circuit briefly described in Chapter III is typical of its kind and is reproduced above in Fig. 37.

A triggering pulse of 200V from the event selection circuits causes the thyratron to strike, so that the anode potential collapses rapidly from V (the E.H.T. Supply) to earth potential.

The condenser C_1, charged to a potential V, suddenly has one terminal earthed via the low impedance of the thyratron causing it to share its charge with the spark chamber capacity C_c via the resistance R_c. Thus a pulse of amplitude $V\frac{C_1}{C_1+C_c}$ with a rise time $T_R = \frac{C_1 C_c}{C_1+C_c} R_c$ is applied to the chamber. If no spark appears in the chamber this voltage will decay with a time constant $T_{Decay} = R\ (C_1+C_c)$, but as soon as a spark is formed the voltage across the chamber will collapse very rapidly through the conduction filament of the spark channel (e.g. see Fig. 9). If $C_1 \gg C_c$, $T_R = C_c R_c$ and $T_{Decay} = R_1 C_1$. Typical values of R_1 and C_1 are 100Ω and 0.001 μF respectively.

It is essential that the rise time of the high voltage pulse be less than the spark formation time, otherwise it may be possible for the initial electrons to be cleared out of the gap by the rising edge of the pulse before the avalanches have a chance to develop. This means that rise times of approximately 20 nsec are required.

For a typical chamber of n gaps of electrode area 500 cm^2 and gap width 1 cm the capacity per gap is ~50pF. Since the electrodes are connected in parallel $C_c \sim 50n$ pF. Thus, if the condition $R_c C_c \sim 20 \times 10^{-9}$ sec is to be satisfied, $R_c \sim 400/n$ ohms. At an operating voltage of V = 10 kV, the maximum current required from the high voltage trigger is therefore 10,000n/400 = 25n amps. Such currents may be obtained only with hydrogen thyratrons or triggered spark gaps.

The most popular hydrogen thyratron is the 5C22 and high voltage pulse generator circuits employing this valve have been described by Fischer and Zorn (1961), and Meyer and Terwillinger (1961). With a grid drive of 400V amplitude obtained from an EFP60 secondary emission valve the above authors obtained a minimum delay time of 0.1 μsec in the striking of the thyratron.

Triggered spark gaps have the advantage that they are both faster and cheaper (the delay time is ~0.02 μsec). The disadvantage is that they require a triggering voltage of ~5kV which may be obtained from either a pulse transformer, or a small fast thyratron like the 3C45, whose delay time is ~0.04 μsec.

5.3 The connections to the spark chamber electrodes

It has been observed by many workers that small variations in gap spacing can result in large variations in gap efficiencies and spark intensities. The reason for this is that the rapid collapse of the high voltage pulse occurs when the impedance of a discharge streamer becomes comparable with the source impedance. Less rapidly developing streamers in slightly bigger gaps may be so retarded in their development that they are unable to give rise to a spark before the high voltage collapses, or, at best, they may only give rise to a comparatively faint spark. To avoid this, it is desirable to have as low a source impedance as possible so that each spark has as long a time as possible in which to develop.

Another way of minimising this effect is to decouple the high voltage plates either (a) by providing each with its own storage capacitor, or (b) by connecting each high voltage plate through a small decoupling impedance R_c to a single capacitor C_1 as shown in Fig. 37. In this way the high voltage plates do not have a common source impedance and interaction between them is reduced. A further advantage of method (b) is that R_c protects the thyratron against excessive currents. Since the impedance of the conducting thyratron itself is very low, it is unnecessary to provide a separate thyratron for each gap, although Fischer and Zorn (1961) have used five 5C22 output thyratrons triggered simultaneously by a 3C45 thyratron.

If the high voltage pulse generator can be placed close to the chamber, then the decoupling impedance R_c may be a resistor of appropriate magnitude for the required rise time, i.e. of the order of 10-100Ω. If it is not practicable to place the high voltage pulse generator beside the chamber, a low impedance cable may be used to connect R_c to the chamber. It was found in the present experiment that the former method produced much "cleaner" pulse shapes than the latter, which caused a certain amount of oscillation in the pulse, presumably due to the stray capacitance and inductance of the cable. A method favoured by Rutherglen (1963) is to feed the high voltage pulse separately to each gap through cables more than 2 metres long, so that the transit time along them was about 10^{-8} sec thus providing quite adequate isolation of

the plates.

Rutherglen found standard cables of characteristic impedence in the range 50-100Ω suitable for this purpose.

5.4 The gas filling

Spark chambers are normally filled with neon, helium, argon, or a mixture of these gases. The relative advantages and disadvantages of neon, argon and henogal (65% Ne, 34% He), which are the fillings most commonly used, will be considered in this section.

Neon works satisfactorily with an applied pulse in the range 6-10 kV/cm. It is considered by most workers to be the most suitable gas for the recording of multiple tracks. Welder's grade neon (98% Ne, 2% He), which was used in the experiments described in this thesis, is of quite adequate purity; it is to no real advantage to use research grade neon which is much more expensive. A liquid nitrogen trap may be used to freeze out impurities (such as oxygen and water vapour) during the filling process because neon liquefies at -246°C. The sparks obtained with neon are very bright and the variation in the light intensity of sparks in neon is relatively small compared with sparks in other gases. The spark formation time of neon is slightly less than that of Helium, and an order of magnitude less than that of argon. The only real disadvantage of neon is the price, which is ten shillings per litre in the U.K. For chambers not constructed to withstand evacuation this presents a serious

financial handicap, because they must be filled by flowing neon through the chambers displacing the air until a negligible amount of air impurity remains inside it. For a remainder of 0.01% air the volume of neon which must be used is nearly ten times that of the chamber.

The main advantage of argon is that it is very cheap at 7d. per cu. ft., or $\frac{1}{4}$d. per litre. Argon is thought to be an unsatisfactory gas for recording multiple tracks. A typical operating voltage for argon is ~16kV/cm. Argon liquefies at -185°C and oxygen at -182°C, and therefore it is not possible to separate them by liquefaction.

Henogal is fairly expensive at approximately seven shillings per litre in the U.K. It is used to a large extent by the groups at CERN, Geneva, who can obtain it for as little as 2d/litre. It has a lower operating voltage than argon, and is suitable for the recording of multiple tracks. The sparks, red in colour, are not as bright as those obtained with argon or neon. The CERN group have considered first filling the spark chambers with CO_2 to avoid the great loss of filling gas. The CO_2 is then relatively easily removed by trapping it in liquid nitrogen, henogal replacing it at the same rate as the CO_2 is removed. This cannot be done with argon because the efficiency drops below 50% for A-CO_2 mixtures containing less than 1% CO_2. The cost saved by this method for argon is, however, negligible because argon is so cheap.

Some workers use neon +0.1% argon, which has the lowest

operating voltage of all mixtures. This is explained by the Penning effect (see Druyvesteyn and Penning, 1940). With neon alone in the course of the avalanche the electrons produce ionisation which gives rise to a multiplication of the electrons, but frequently the electrons raise neon atoms to an excited state which does nothing to reproduce electrons. If a small amount of argon is added the reaction $Ne^* + A \rightarrow A^+ + e^- + Ne$ takes place, i.e. excited neon atoms (excitation potential 15.8V), which are produced in large numbers at low electric fields, ionise neutral argon atoms by collision, thereby causing a greater rate of reproduction of electrons with a subsequent decrease in breakdown voltage.

In section 4.1d it has been reported that the addition of small amounts of alcohol or other impurity was found to cause severe increases in the drift velocities of electrons in neon, argon, and helium fillings. Alcohol is often introduced to the chamber for this reason, because the increase of the electron drift velocity will reduce the sensitive time in a clearing field, although it is then not possible to predict exactly the magnitude of clearing field required to produce a specific sensitive time. Many workers (the author included) have also observed that the addition of alcohol reduces the probability of spurious breakdown.

From Fig. 33 it may be seen that the presence of comparatively large amounts of electronegative impurity seriously decreases the efficiency of the chamber. O'Neill (see Rutherglen, 1963) has suggested that this presents an alternative method of controlling the

sensitive time of a spark chamber when the use of an electric field is not desirable. An example of this is a spark chamber operated in a magnetic field parallel to the plates where a D.C. clearing field would cause a displacement of sparks from the particle trajectory proportional to the produce $\underline{E} \times \underline{B}$.

5.5 Methods of Photography

Spark chamber tracks are normally recorded photographically by using a camera with an open shutter pointing at the chamber in a dark enclosure.

The amount of light emitted by a spark depends on the nature of the filling gas used and the operating voltage, longer over-voltages producing brighter sparks. Generally speaking, apertures in the range of f/4 to f/11 are suitable for obtaining a satisfactory record of particle tracks on fast panchromatic film such as Kodak Tri-X or Ilford HPS.

Normally it is arranged for a relay circuit to wind the camera on automatically after each event, and the chamber is prevented from functioning again until the camera has stopped winding. If it is necessary to make full use of the fast recovery time of the spark chamber ($\simeq$10 msec) a camera with a very fast film transport mechanism is required, such as a cine camera adapted for single frame operation.

To determine the position of the track of a particle in terms of two coordinates stereo photographs are required, the two views

normally being inclined at a right angle to one another. It is customary, if practicable, to record the two stereo views on the same negative by the use of a mirror. The optical path lengths from the sensitive volume of the chamber to the camera lens will then be different for the two stereo views. If the depth of field of the camera lens at its required aperture is inadequate a multiple mirror system, an example of which is described by Cronin and Renninger (1960), must be employed. If the coordinates of more than one simultaneous particle track are to be measured stereoscopically, a third view is normally recorded to resolve ambiguities. For the measurement of tracks with respect to some experimental coordinate system it is convenient to photograph reference lines with each track. These could be accurately inscribed on the chamber walls.

In a multi-gap parallel plate spark chamber it is not possible for one camera lens to cover the entire sensitive volume of each gap. For a small chamber the camera maybe placed at a long distance away from it to cover as much of each gap as is required. The limit to the distance is set by the intensity of the sparks and the image size on the negative. As the dimensions of the plates are increased it becomes more and more difficult to arrange for a satisfactory compromise between the short focal length required to obtain the necessary depth of field and the long focal length required to obtain an adequately sized negative image.

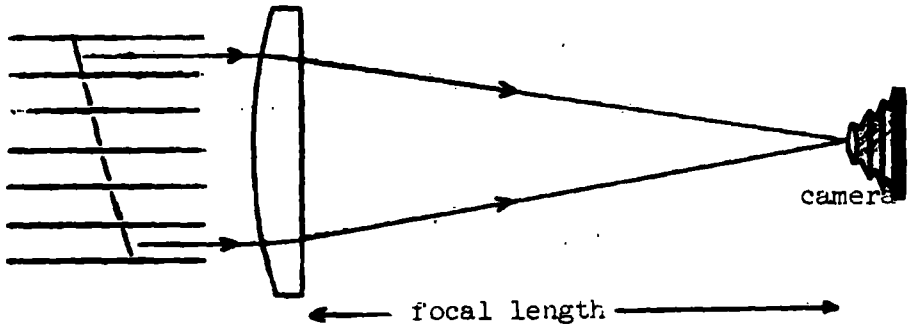

(a)

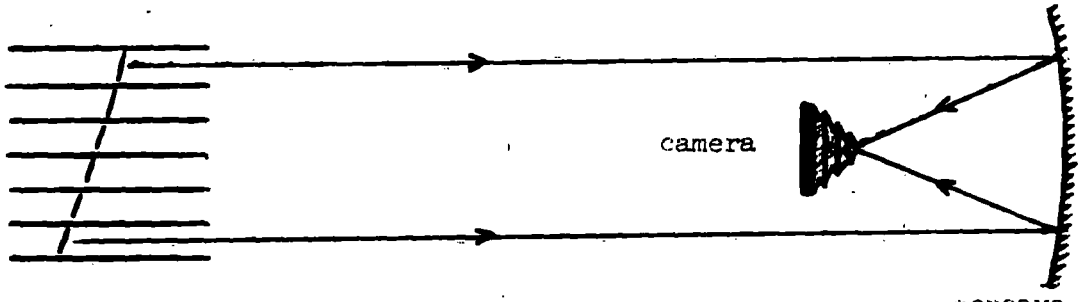

(b)

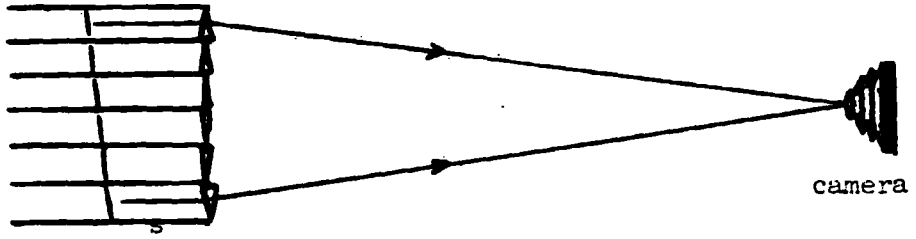

(c)

Fig. 38. Three methods of photography.

If the chamber contains a large number of gaps they may be arranged fan-wise so that their central planes pass through the camera lens. This is particularly convenient if the chamber has been constructed of individual units as described in §5.1.

Three possible methods are: to place a cylindrical lens in front of the chamber so that the camera lens is positioned at its focal point, as shown in Fig. 38a, to use a spherical concave mirror as shown in Fig. 38b, or to use small angle refracting prisms as shown in Fig. 38c. The distortion introduced by these optical aids may be allowed for in accurate track measurements.

Finally, it is desirable for the images of the sparks to be as narrow as possible for accurate measurements. The use of a fine grain film and slight underexposure with overdevelopment would help to achieve this, but neither method is really practicable. Fine grain films will not, in general, be sufficiently sensitive to record the sparks, particularly if the camera is at a large distance from the chamber, and underdevelopment would cause comparatively faint sparks to be cut off.

CHAPTER VI

A Survey of the different types of spark chamber developed up to the present time

Various types of spark chamber, differing from the conventional parallel plate design, have been developed for particular purposes. In this chapter the relative advantages of the various types will be briefly considered.

6.1 Wire Spark Chambers

The track of a curved particle trajectory in a parallel plate spark chamber will be recorded with maximum accuracy when it is normal to the plates, and with minimum accuracy when it is at small angles to the plates.

Mann (see Romanowski, 1961) suggested that a method of accommodating high curvatures accurately in a given plane was to build a spark chamber whose electrodes were constructed of parallel wires or rods, the direction of the wires in alternate layers being at right angles to one another and the ends of the rods forming a rectangular lattice. Ramanowski (1961) reports the construction of such a chamber made of parallel wires $\frac{1}{16}$ in. in diameter spaced $\frac{1}{4}$ in. apart. With alternate wires in the same layer pulsed and earthed most of each wire's nearest neighbours are at opposite polarity to it.

Such a chamber has a preferred plane of optimum accuracy normal to the wires as compared to a preferred axis, normal to the plates, in a parallel plate spark chamber. This is an important advantage in viewing the curved trajectory of a particle in a magnetic field:- if the wires are normal to the magnetic field direction, the entire particle trajectory, even if it describes a complete circle, is equally amenable to accurate measurement.

A further advantage is that the sparks can be photographed through the electrodes.

The biggest single advantage, however, is probably the fact that such a chamber can be used to obtain digitized information about the track position directly thus eliminating the use of photographic film as a storage medium with obvious saving in scanning time and cost.

Aucamp et al. (1963) have described an elegant method of constructing individual spark chamber units consisting of one aluminium plate electrode and a wire grid machined on the copper foil of a printed circuit board. The problem of maintaining sufficient tension in the wires of a wire-chamber is thus eliminated. Several such units can be combined to form a multi-layer spark chamber.

Some preliminary results on the use of ferrite memory cores to provide digital electronic read-out suitable for high speed electronic analysis have been reported by Krienen (1963). The

current pulse associated with a spark is registered by a ferrite core threaded on the wire to which the spark jumped. This information is stored directly in a magnetic memory for further processing.

Ancamp et al. (1963) have investigated the accuracy of track location. They conclude that the position of a switched core in the memory determines the position of the track to an accuracy of better than 1 mm for a spacing between the wires of 1 mm.

Krienen claims that it should eventually be possible to achieve read-out times of the same order of magnitude as the recovery time of the chamber.

6.2 Sonic Spark Chambers

The fact that sparks produce a cracking sound induced Fulbright and Kohler (1961) to build the first sonic spark chamber. The principle of operation is based on the measurement of the time delay between the occurrance of the spark and the receipt of the sound wave emitted by it at a number of acoustic probes.

The time of flight of the sound, as measured by two piezoelectric transducers a certain distance apart, serves to define the spark position uniquely. The tips of the probes are hemispherical to ensure that the time of flight measurement is independent of the angle of incidence of the sound wave.

Maglić (1963) reported a spatial resolution of 0.8 mm. His acoustic probes had a relatively long recovery time of ~10 msec due to oscillations caused by internal reflections inside the chamber and wave-guides leading from it, which meant that two probes per gap could only resolve one single particle track.

An important development by Whitehead (see Maglić, 1963) removed this limitation. By using probes without wave-guides and damping them with an acoustically matched substance (tungsten loaded with araldite) he was able to reduce the recovery times to ~10 μsec. With three such probes per gap any number of sparks may be resolved provided that they are separated by a distance greater than 3 mm. With these probes an event may be recorded every 1-2 msec, and the limitations are now set by the recovery time of the spark chamber and the speed with which the recording system can assimilate the data.

The sonic spark chamber avoids the use of lenses and mirrors, and eliminates the need for the taking, scanning, and measurement of photographs by obtaining the data in a digitized form.

Charpak (1962) constructed a chamber with special electrodes having the nature of a distributed delay-line. He was able to determine the initial position of the spark by measuring the delay between the arrival of the signal following the spark at two opposite ends of the electrodes. By this method one should be able to locate the position of the track to within 1 mm, within a time shorter than 1 μsec. This fact is of particular interest

if one wants to use the information provided by such a chamber to trigger other spark chambers.

The three types of digitised spark chamber described above combine the short time resolution and high spatial accuracy, which are associated with all types of spark chamber, with a high speed data analysis.

6.3 Cylindrical Spark Chambers

Fig. 39 shows a cylindrical spark chamber constructed by the Berkeley group (Beall et al., 1963) for an experimental study of K^--p interactions in the momentum range 700 to 1400 MeV/c.

Large solid angle and high angular resolution were obtained by surrounding the 6 in. wide liquid hydrogen target with the tengap cylindrical chamber. The electrodes were made of 0.010 in. thick aluminium foil cylinders 18 in. long, varying in diameter from 10 to 20 in. They were supported at the end in two polished perspex end plates. The gap width was 0.375 ± 0.010 in.

Another semi-circular chamber was placed behind the target to measure the range and polarisation of certain of the reaction products. This contained 21 two-gap spark chambers interleaved with 12 1 in. thick carbon absorbers at radii ranging from 18 to 40 in. The whole assembly measured 5 x 6 x 3 ft^3 and weighed six tons.

To define the incident momentum of the K^- meson in the Bevatron beam to within $\pm$ 0.5% two small spark chambers with 0.003 in. thick

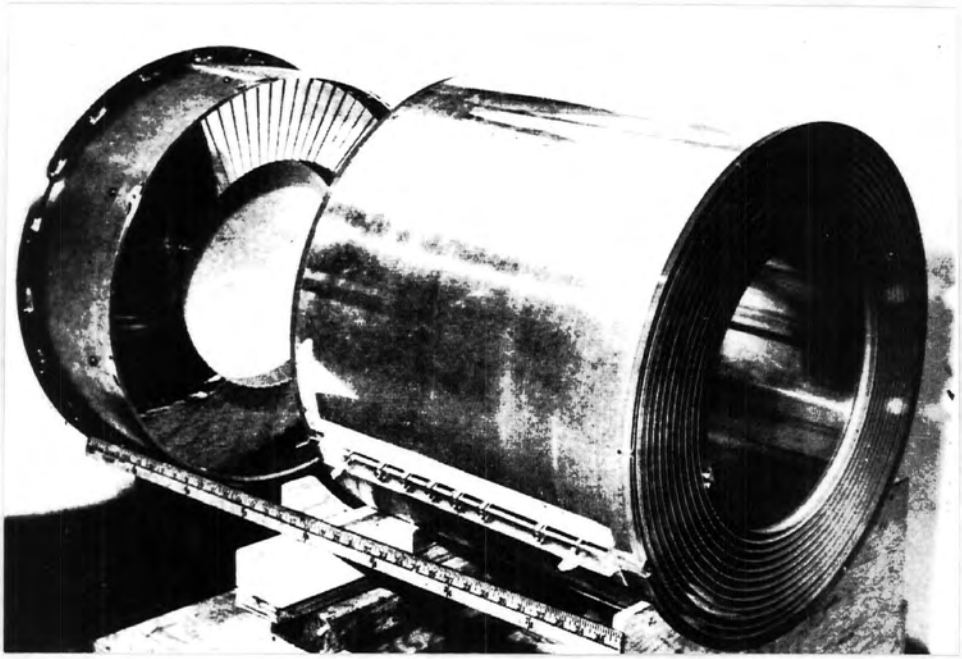

Figure 39. Cylindrical chamber constructed by the Berkeley group. The segmented mirror is shown at the left.

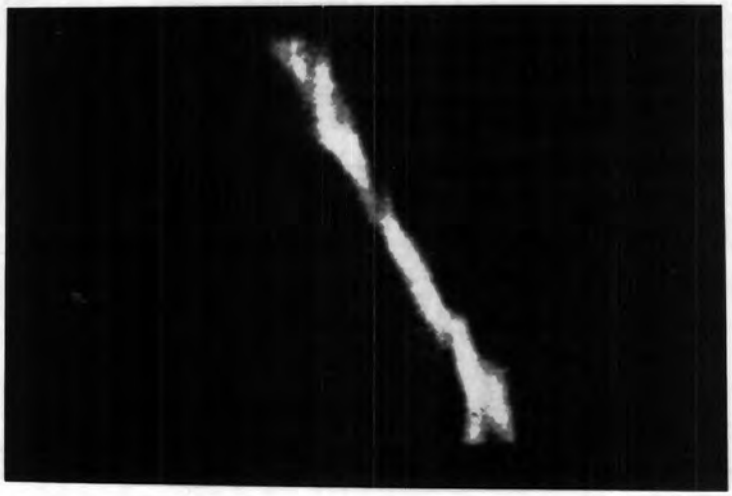

Figure 40. Typical cosmic ray track obtained with a microwave spark chamber.

foil electrodes were used on either side of a bending magnet.

The chambers were filled with a mixture of 10% helium and 90% neon and operated in a clearing field of 35 V.

Depth and angular information was aquired by the use of tilted mirrors behind the cylindrical chamber (see fig. 39). The mirror segments were arranged almost radially on a machined perspex plate and were tilted at an angle of 5.7° to a plane normal to the axis of the cylindrical electrodes thereby providing an effective stereo veiwing angle of 11.4°.

Kaftanov and Liubimov (1963) have described a six-gap cylindrical spark chamber, filled with neon, used in experiments on $\mu \rightarrow e+\gamma$ and $\mu \rightarrow 3e$ decay modes.

The advantage of cylindrical chambers is that they can completely surround the garget thus both achieving a large detection solid angle and minimising loss corrections for the decay of short-lived particles.

6.4 Microwave Spark Chambers

Microwave spark chambers, in which a pulsed microwave field is applied to the chamber, were developed in an attempt to make the spark discharge follow the particle trajectory rather than the applied field direction.

Work on microwave spark chambers has been reported by Fukui et al. (1960), Ledermann (1961), and Fukui et al. (1963).

Fukui et al. (1960) found that in order to obtain a visible track of 1 mm width, the pulsed microwave field should be applied within 2 μsecs of the transit of the particle, and the field strangth should be a few times greater than that required for breakdown with a duration of 0.1 μsec.

Fukui et al. inserted the sensitive volume, a glass tube filled with the gas mixture (Ne + 1%A + 0.4% HCO OC_2 H_5 at 500 mm Hg pressure), in a wave guide along which the microwave pulse was transmitted to be absorbed into a dummy load. Lederman used a resonant gas-tight cavity filled with argon. Fig. 40 shows a typical cosmic ray track obtained by Fukui et al. (1963). The uniformity of the field is an essential factor for the production of very fine tracks. For this reason the former method is preferable because a resonant cavity produces a non-uniform field.

6.5 Spark Chambers in Magnetic Fields

A system of spark chambers in a magnetic field effectively becomes a new type of visual track detector. It combines the advantages of the magnetic field - momentum and sign determination- with those of the spark chamber, namely the ability to accurately define particle trajectories, to observe decays and interactions, to tolerate high particle fluxes, and to permit electronic selection of events if desired.

The Princeton (O'Neill et al., 1963) and Argonne (Burleson et al., 1963) groups have been responsible for the main part of

the development of magnetic field sparkchambers of high resolution. Full details of this work are reported by O'Neill et al. (1963) and Burleson et al. (1963), and an indication of the large degree of success with which this work has met is given by the frontispiece, which shows electron cascades produced in a spark chamber in a magnetic field of ±13.5 kG.

Acknowledgments

The author wishes to thank the National Institute for Research in Nuclear Science for sponsoring this work, and the Department of Scientific and Industrial Research for the award of a grant. He is indebted to Professor G.D. Rochester, F.R.S., for his interest in the work and the use of his laboratory facilities; to his supervisor Dr. A.W. Wolfendale for his unfailing guidance and to Dr. M.G. Thompson for his continual help and advice. Finally he is indebted to the laboratory staff of the Physics Department, especially to Mr. R.L. Stark, whose assistance was invaluable.

References

Alikhanian, A.I., and Kozodaev, M.S., 1960, International Conference on Instrumentation for High Energy Physics, Berkeley (New York: Interscience), p. 174.

Allkofer, O.C., 1959, Atomkernenergie, 4, 169.

Allkofer, O.C., 1960, Zeit, Phys., , 274.

Allkofer, O.C., Bagge, E., Henning, P.G., and Schmieder, L., 1957, Atomkernenergie, 2, 88.

Aucamp, A.L., Koen, J.W., Meyer, M.A., Van Der Walt, J.J., and Wolmarans, N.S., 1963, private communication.

Bagge, E., and Allkofer, O.C., 1957, Atomkernenergie, 2, 7.

Bagge, E., and Schmieder, L., 1957, Atomkernenergie, 4, 389.

Beall, E.F., Cork, B., Murphy, P.G., and Wenzel, W.A., 1960, International Conference on Instrumentation for High Energy Physics, Berkeley (New York: Interscience), p.277.

De Beer, J.F., 1960, thesis, University of Potchefstroom, South Africa.

Bella, F., and Franzinetti, C., 1953a, Nuovo Cim., 10, 1335.

Bella, F., and Franzinetti, C., 1953b, Nuovo Cim., 10, 1338.

Bella, F., Franzinetti, C., and Lee, D.W., 1953, Nuovo Cim., 10, 1461.

Bowe, J.G., 1960, Phys. Rev., 117, 1411.

Brown, S.C., and Allis, W.P., 1958, Basic Data of Electrical Discharges, M.I.T. Tech. Report, 283.

Burleson, G.R., Hoang, T.F., Kalmus, P.I.P., Kuskowski, R.L., Niemela, L.W., Roberts, A., Romanowski, T.A., Warshaw, S.D., and Yurka, G.E., 1963, Nucl. Inst. Methods, 20, 180 and 185.

Burleson, G.R., Roberts, A., and Romanowski, T.A., 1961, Rev. Sci. Instr., 32, 1069.

Burnham, J.U., Rogers, I.W., Thompson, M.G., and Wolfendale, A.W., 1963, J. Sci. Instrum., 40, 296.

Chang, W.Y., and Rosenblum, S., 1945, Phys. Rev., 67, 222.

Charpak, G., 1962, Nucl. Inst. Methods, 15, 318.

Compton, K.T., and Langmuir, I., 1930, Rev. Mod. Phys., 2, 193.

Conversi, M.M., Focardi, S., Franzinetti, C., Gozzini, A., and Murtas, P., 1956, Nuovo Cim. Suppl., 4, 234.

Conversi, M.M., and Gozzini, A., 1955, Nuovo Cim., 2, 189.

Cork, B., 1961, Rev. Sci. Instrum., 32, 486.

Coxell, H., and Wolfendale, A.W., 1960, Proc. Phys. Soc., 75, 378.

Cranshaw, T.E., and De Beer, J.F., 1957, Nuovo Cim., 5, 1107.

Cronin, J.W., 1961, Rev. Sci. Instrum., 32, 487.

Cronin, J.W., and Renninger, G., 1960, International Conference on Instrumentation for High Energy Physics, Berkeley (New York: Interscience), p. 271.

Culligan, G., Harting, D., and Lipman, N.H., 1960, CERN Report 61-25.

Daion, M.I., Volinskii, V.K., and Potapov, L.I., 1960, see Alikhanian and Kozodaev.

Danby, G., Gaillard, J.M., Goulianos, K., Lederman, L.M., Mistry, N., Schwarz, M., and Steinberger, J., 1962, Phys. Rev. Letters, 9, 36.

Dickey, F.B., 1952, J. Appl. Phys., 23, 1336.

Druyvesteyn, M.J., and Penning, F.M., 1940, Rev. Mod. Phys., 12, 87.

Von Engel, A., 1955, Ionised Gases (Oxford: Clarendon Press).

Fischer, J., and Zorn, G.T., 1961, Rev. Sci. Instrum., 32, 499.

Fukui, S., Hayawaka, S., Tsukishima, T., and Nukushina, H., 1960, International Conference on Instrumentation for High Energy Physics, Berkeley (New York: Interscience), p. 267.

Fukui, S., Hayawaka, S., Tsukushima, T., and Nukushina, H., 1963, Nucl. Inst. Methods, 20, 236.

Fukui, S., and Miyamoto, S., 1959, Nuovo Cim., 11, 113.

Fukui, S., and Miyamoto, S., 1961, J. Phys. Soc. Japan, 16, 2574.

Fulbright, H.W., and Kohler, D., 1961, University of Rochester Report NYO-9540.

Glaser, D.A., 1952, Phys. Rev., 87, 665.

Greinacher, H., 1936, Helv. Phys. Acta, 9, 520.

Henning, P.G., 1955, thesis, Hamburg University, Germany.

Heyn, M.P., 1961, thesis, Princeton University, U.S.A.

Kaftanov, V.S., and Liubimov, V.A., Nucl. Inst. Methods, 20, 195.

Keuffel, J.W., 1948, Phys. Rev., 73, 531.

Keuffel, J.W., 1949, Rev. Sci. Instrum., 20, 202.

Krienen, F., 1963, Nucl. Inst. Methods, 20, 168.

Kruithoff, A.A., and Penning, F.M., 1937, Physica, 4, 430.

Lederman, L.M., 1961, Rev. Sci. Instrum., 32, 523.

Lloyd, J.L., 1960, Proc. Phys. Soc., 75, 387.

Madansky, L., and Pidd, R.W., 1948, Phys. Rev., 73, 1215.

Madansky, L., and Pidd, R.W., 1949, Phys. Rev., 75, 1175.

Madansky, L., and Pidd, R.W., 1950, Rev. Sci. Instrum., 21, 407.

Maglić, B.C., 1963, Nucl. Inst. Methods, 20, 165.

Meek, J.M. and Craggs, J.D., 1953, Electrical Breakdown in Gases (Oxford University Press).

Meyer, D.I., and Terwilliger, K.M., 1961, Rev. Sci. Instrum., 32, 512.

Mistry, N.B., Murthy, G.T., Ramana Murthy, P.V., and Sreekantan, B.V., 1960, Nuovo Cimento, 17, 429.

O'Neill, G.K., 1961, Rev. Sci. Instrum., 32, 528.

O'Neill, G.K., Murphy, F.V., Wright, K., and Yount, D., 1963, Nucl. Inst. Methods, 20, 176.

Roberts, A., 1961, Rev. Sci. Instrum., 32, 482.

Romanowski, T.A., 1961, Rev. Sci. Instrum., 32, 516.

Rutherglen, J.G., 1963, private communication, to be published in Prog. Nucl. Phys., 9.

Rutherglen, J.G., and Paterson, J.M., 1961, Rev. Sci. Instrum., 32, 519.

Sayers, A., 1938, Proc. Roy. Soc. A, 169, 83.

Schneider, F., and Höhne, K.H., 1963, Nucl. Inst. Methods, 20, 152.

Trümper, J., 1960, Atomkernenergie, 4, 121.

Wilson, R., 1950, Phil. Mag., 41, 66.